

Global sensitivity analysis informed model reduction and selection applied to a Valsalva maneuver model

E. Benjamin Randall^{a,b,*}, Nicholas Z. Randolph^a, Alen Alexanderian^a, Mette S. Olufsen^{a,**}

^a*Department of Mathematics, North Carolina State University, Raleigh, NC*

^b*Department of Molecular and Integrative Physiology, University of Michigan, Ann Arbor, MI*

Abstract

In this study, we develop a methodology for model reduction and selection informed by global sensitivity analysis (GSA) methods. We apply these techniques to a control model taking systolic blood pressure and thoracic tissue pressure data as inputs, predicting heart rate in response to the Valsalva maneuver (VM). The study compares four GSA methods based on Sobol' indices (SIs) quantifying parameter influence on the difference between the model output and the heart rate data. The GSA methods include standard scalar SIs determining the average parameter influence over the time interval studied and three time-varying methods analyzing how parameter influence changes over time. The time-varying methods include a new technique, termed limited-memory SIs, predicting parameter influence using a moving window approach. Using the limited-memory SIs, we perform model reduction and selection to analyze the necessity of modeling both the aortic and carotid baroreceptor regions in response to the VM. We compare the original model to three systematically reduced models including (i) the aortic and carotid regions, (ii) the aortic region only, and (iii) the carotid region only. Model selection is done quantitatively using the Akaike and Bayesian Information Criteria and qualitatively by comparing the neurological predictions. Results show that it is necessary to incorporate both the aortic and carotid regions to model the VM.

Keywords: Mathematical modeling, Sobol' indices, Time-dependent processes, Akaike Information Criterion, Bayesian Information Criterion

*Corresponding author

**Principal corresponding author

Email addresses: ebrandal@umich.edu (E. Benjamin Randall), nzrandol@ncsu.edu (Nicholas Z. Randolph), aalexan3@ncsu.edu (Alen Alexanderian), msolufse@ncsu.edu (Mette S. Olufsen)

Abbreviations

In order of appearance:

Systolic blood pressure	SBP
Intrathoracic pressure	ITP
Valsalva maneuver	VM
Local sensitivity analysis	LSA
Global sensitivity analysis	GSA
Quantity of interest	QoI
Sobol' indices	SI _s
Pointwise-in-time Sobol' indices	PTSI _s
Generalized Sobol' indices	GSIs
Limited-memory Sobol' indices	LMSI _s
Akaike information criterion with correction	AIC _c
Bayesian information criterion	BIC
Delay differential equations	DDE
Electrocardiogram	ECG
Piecewise cubic Hermite interpolating polynomial	PCHIP
Respiratory sinus arrhythmia	RSA
Ordinary differential equations	ODE
Standard deviation	SD
One-at-a-time analysis	OTA
Initial conditions	IC _s

1. Introduction

Mathematical models describing cardiovascular processes are typically complex with many nonlinear interactions. The level of detail necessary to explain these interactions varies with the type of system studied and the questions investigated. Such models with many interrelated states can be difficult to analyze and parameter values difficult to assign, especially with limited data to inform the model. Simplifying or reducing such models may facilitate model-based data analysis provided that the reduced model retains similar behavior to the original. Though formal model reduction methods exist [3], they typically focus on analyzing model input-output relationships, ignoring predicted quantities for which there is no available data. Moreover, these techniques identify one reduced model when in fact many reduced models can be generated. In this study, we develop a systematic approach for model reduction and selection via global sensitivity analysis. We apply this protocol to our model [35] that uses systolic blood pressure (SBP) and intrathoracic tissue pressure (ITP) data as inputs to predict heart rate responses to the Valsalva maneuver (VM). We use model selection to investigate if it is necessary to differentiate between the aortic and carotid baroreceptor afferent signals in the model and determine which compartments should be modeled.

The VM is conducted by forcefully exhaling against a resistance [46]. The VM stimulates the baroreceptor reflex (*baroreflex*) triggered by the deformation of baroreceptors in the aortic arch and carotid sinus. These receptors sense changes in blood pressure initiating a signal cascade transmitted through parasympathetic (vagal) and sympathetic neurons controlling heart rate, vascular resistance, vascular compliance, and cardiac contractility [46]. In healthy adults, these signals maintain homeostatic heart rate and blood pressure; however, in disease they can become impaired. To understand how to treat patients with impaired autonomic function, it is essential to know how the signals are impacted. To trust model predictions, it is prudent to use a well-validated model in which parameters can be estimated uniquely when comparing the model output to data.

To effectively perform optimization, we estimate parameters that are most influential to the model output. We employ *local* (LSA) or *global* (GSA) sensitivity analysis techniques determining the influence of the model parameters on a quantity of interest (QoI). LSA (e.g., [7, 27, 30]) compute partial derivatives of the QoI with respect to the parameters, perturbing them one at a time about a known “local” value, quantifying the effect of each parameter without accounting for parameter interactions. GSA methods [38] compute parameter influence by analyzing parameters and their interactions over the entire prescribed parameter space. Popular GSA methods include Sobol’ indices (SIs) [41] (used in this study), Morris screening [28, 29], generalized sensitivity functions [16], and moment-independent importance measures [14]. Morris screening is computationally inexpensive, but results are first-order approximations that do not account for higher order interactions [28]. Generalized sensitivity functions characterize the sensitivity of a model to nominal parameter values and take into account parameter interactions; however, they make more stringent assumptions on local parameter identifiability [16]. Moment-independent importance measures focus on constructing probability density functions for the QoI that are computationally expensive but intractable for larger systems [14].

We compute GSA using SIs [37, 41] due to their ease of calculation and wide usage [6, 18, 22, 44]. SIs apportion relative contributions of the overall effect on the QoI to each parameter. They were originally developed to analyze parameter influence in models with scalar outputs [41] (referred to here as *scalar* SIs) but have recently been extended to analyze time-varying QoIs [1]. One way to compute time-varying SIs is to calculate the index at every time point [2, 18] (referred to here as *pointwise-in-time* Sobol’ indices (PTSIs)). This approach is simple but neglects the time correlation structure and history of the model output. To solve this problem, Alexanderian et al. [1] proposed a method incorporating time dependence, termed *generalized* Sobol’ indices (GSIs),

that have many applications for models with time-dependent outputs. However, for simulations that involve significant, short-lived disturbances to the steady-state behavior within the time course of interest, integration over the entire time interval can average the effects of model parameters, diminishing features that only play a role during short time intervals. We illustrate this point using our VM model, where the breath hold causes a substantial yet transient model response. To mitigate these effects, we propose a new method referred to here as *limited-memory* Sobol’ indices (LMSIs). These indices account for parameter interactions, time correlations, and a snapshot of the history of the variance by applying weights from a moving window of width $\Delta < T$ for T the length of the time interval.

In addition to sensitivity analysis, we propose a methodology for model analysis, reduction, and selection. For model reduction, we employ the LMSIs to select parameters that are noninfluential over the entire time interval. These parameters are “removed” using one of two processes: (i) by excision of the mathematical equation(s) associated with the noninfluential parameter [7, 26]; or (ii) by fixing the noninfluential parameter at its nominal value [41]. The former approach changes the structure of the model. This process generates a set of reduced models, upon which we perform model selection using the Akaike Information Criterion with correction (AICc) and Bayesian Information Criterion (BIC) [47]. Finally, we determine if the reduced models can predict heart rate and autonomic responses to the VM.

In summary, new contributions of this article include: (i) the development of LMSIs for time-dependent processes incorporating a moving window to resolve the transient nature of the VM; and (ii) a model reduction and selection protocol informed by the LMSIs. These methods are illustrated using our model predicting the heart rate response to VM [35]. Finally, we use model selection to test the need for including afferent signaling from the carotid region only, the aortic region only, or both regions simultaneously when predicting heart rate dynamics.

This study is organized as follows: Section 2 describes the VM; Section 3 presents the mathematical methods, including the LMSIs, GSA-informed model reduction, and model selection; Section 4 compiles the results of our analyses; Section 5 discusses key findings; and, finally, Section 6 states our conclusions.

2. Valsalva maneuver

The VM is a clinical test involving forced expiration against a closed airway while maintaining an open glottis [11]. It stimulates the parasympathetic and sympathetic nervous systems via the baroreflex in response to blood pressure changes in the aortic arch and the carotid sinus [4]. In an effort to maintain homeostasis, the body responds to a sudden decrease in blood pressure, causing compensatory responses in heart rate, vascular resistance, vascular compliance, and cardiac contractility, which in turn restore blood pressure to baseline. The VM is divided into four phases (illustrated in Figure 1):

- I. Initiation of the breath hold causes a sharp increase in blood pressure and a decrease in heart rate.
- II. Phase II is split into two parts:
 - i. Early phase II - blood pressure drops significantly, triggering parasympathetic withdrawal and accelerating heart rate.
 - ii. Late phase II - delayed sympathetic activation accelerates heart rate further and increases peripheral vascular resistance, which in turn, increases blood pressure.
- III. Release of the breath hold results in a sharp decrease in blood pressure, triggering additional parasympathetic withdrawal.

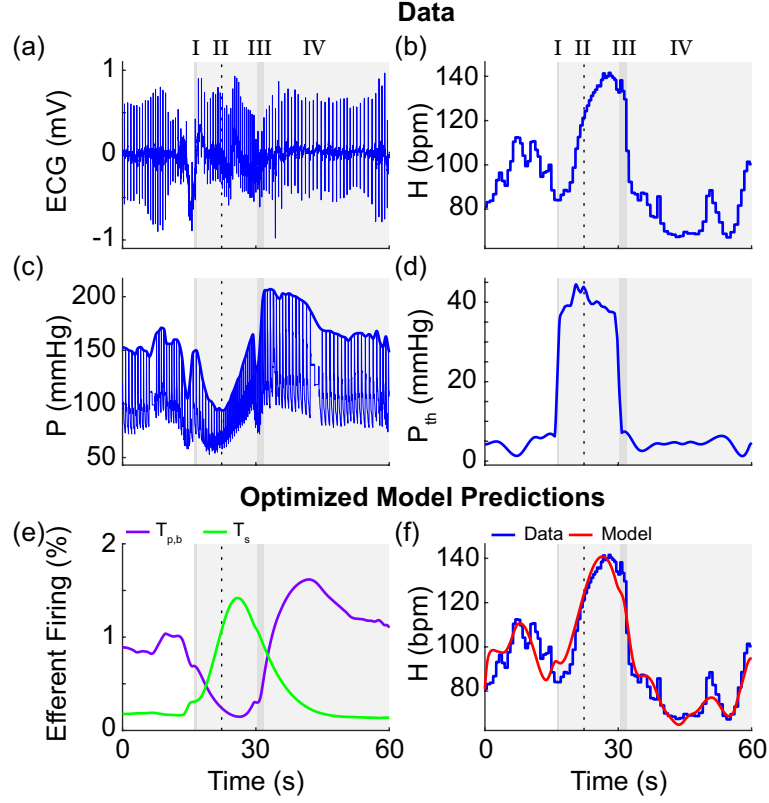


Figure 1: A Valsalva maneuver (VM) for a representative control subject. The VM phases are represented as alternating gray (I and III) and light gray (II and IV) boxes. Phase II is divided into early and late parts (vertical dotted black line). *Data*: (a) Electrocardiogram (ECG, mV). (b) Heart rate (H , bpm). (c) Blood pressure (P , mmHg) with systolic blood pressure (bold) indicated. (d) Thoracic pressure (P_{th} , mmHg) given in equation (2). *Optimized model predictions*: (e) Efferent baroreflex-mediated parasympathetic ($T_{p,b}$, dimensionless, purple) and sympathetic (T_s , dimensionless, green) signals. (f) Heart rate model output (H , bpm, red) fitted to data (blue).

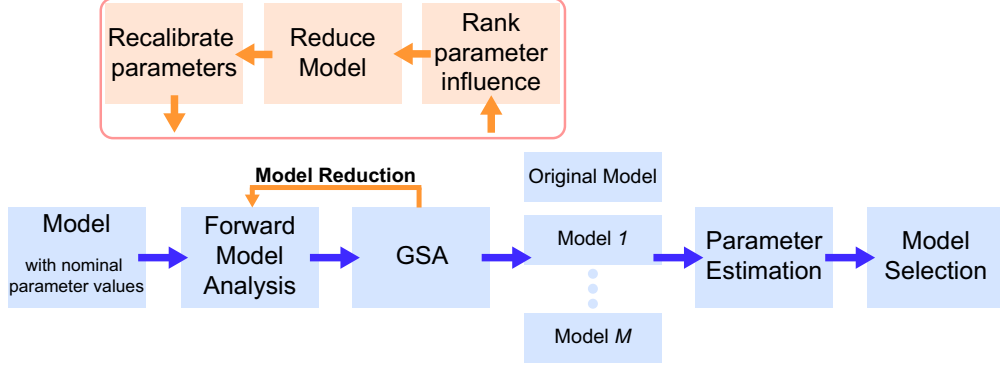


Figure 2: Workflow diagram illustrating the steps in the procedure outlined in Section 3. From left to right: A model is developed and nominal parameter values are determined *a priori*. Forward model analysis produces outputs, quantities of interest, which undergo global sensitivity analysis (GSA). The results from the GSA are used to reduce the model iteratively (orange arrow), producing M reduced models. For each model, a subset of parameters is estimated to fit data. The reduced model that captures the original model best, both qualitatively and quantitatively, is selected. *Iterative Model Reduction Step* (insert): Using GSA, parameters are ranked from the most to the least influential, and parameters below a preset threshold are termed noninfluential. The noninfluential parameters are “removed”, i.e., they can be fixed at their nominal values or the model components associated with these parameters can be analytically removed. Each iteration of this step produces a new reduced model. For each reduced model, nominal parameter values are recalibrated and estimated. Forward model evaluations are conducted and GSA is performed again.

IV. Increased sympathetic activation causes blood pressure to overshoot and return to baseline within 30 s, while normalization of parasympathetic activity gives rise to a sharp drop in heart rate, which subsequently returns to baseline.

3. Methods

We apply the GSA techniques to analyze a system of delay differential equations (DDEs) with 6 states and 25 parameters that takes electrocardiogram (ECG), SBP, and ITP data as inputs and predicts heart rate as the output. Figure 2 depicts the model reduction and selection workflow, which includes the following components:

1. *Forward model analysis* computes the QoI by solving the system with nominal parameter values. In this study, the QoI is the time-varying residual vector

$$\mathbf{r}(t; \theta) = \left[\frac{H_m(t_1; \theta) - H_d(t_1)}{H_d(t_1)}, \dots, \frac{H_m(t_N; \theta) - H_d(t_N)}{H_d(t_N)} \right], \quad (1)$$

where $H_m(t_j; \theta)$ denotes the heart rate model output at time t_j for $j = 1, \dots, N$ and $H_d(t_j)$ denotes the corresponding observed heart rate data. Model predictions depend on the parameter vector $\theta \in \Omega_p \subseteq \mathbb{R}^p$, where Ω_p is the prescribed parameter space of dimension p .

2. *Global sensitivity analysis* determines the influence of the model parameters on the variance of the QoI. We compute scalar SIs with respect to the Euclidean norm of \mathbf{r} ($\|\mathbf{r}(t; \theta)\|_2$) as well as the time-varying PTSIs, GSIs, and LMSIs with respect to \mathbf{r} .
 - (a) *Parameter influence* is computed with the chosen index. We compute LMSIs and determine “noninfluential” parameters as those that have an index that does not exceed a prescribed threshold.
 - (b) *Model reduction* is performed by “removing” noninfluential parameters using one of two approaches:

- i. by fixing noninfluential parameters at their nominal value; or,
 - ii. by analytically removing equations affected by noninfluential parameters.
- (c) *Model recalibration* is required if equations containing noninfluential parameters are modified or removed. This ensures that the reduced model produces similar predictions to the original model.
- (d) *GSA on the reduced model* is conducted (again) to test that all parameter influence indices are above the threshold, i.e., to test if all parameters are influential. This step is necessary since model reduction can cause new parameters to be pushed below the noninfluential threshold.
- Steps (b)-(d) are repeated iteratively until the system has no more noninfluential parameters.
3. *Reduced models*: We create a set $\mathcal{M} = \{m_0, m_1, \dots, m_M\}$, where m_0 is the original model and m_k for $k = 1, \dots, M$ are the reduced models.
 4. *Parameter estimation*: To determine a subset of identifiable parameters ($\hat{\theta}$), we use subset selection analyzing the Fisher Information Matrix as suggested in [26, 29, 30, 33]. A limitation of this method is that it is local in nature, since the model is evaluated at specific parameter values. Each of the reduced models in \mathcal{M} are fitted to data estimating the identifiable influential parameters by minimizing the least squares error between the model predictions and data (the QoI).
 5. *Model selection*: To ensure that the reduced models produce outputs within physiologically acceptable ranges, we perform model selection both quantitatively and qualitatively. Quantitatively, we select the reduced model that best fits the data (heart rate) by calculating relative AICc and BIC values. Qualitatively, we assume the original model is the true signal and compare the outputs (parasympathetic and sympathetic activity) from the reduced models to the original.

3.1. Data acquisition and processing

The data used in this study is measured in a 21-year-old female healthy volunteer following a protocol described in our previous work [35]. Figure 1 displays the collected ECG, blood pressure, and heart rate signals. To determine SBP (Figure 1c) and respiration, we interpolate the local maxima of consecutive blood pressure waveforms in the pulse pressure data and consecutive QRS-complex amplitudes in the ECG data, respectively, via a piecewise cubic Hermite interpolating polynomial (PCHIP) in MATLAB[®] 2019b [35]. This method ensures monotonicity preserving local extrema, since it accounts for both the value of the data and its derivative at each node [8]. Thoracic pressure (P_{th}) combines the measured ITP and the ECG-derived respiration, giving

$$P_{th_j} = \begin{cases} \text{ITP}_j & t_s \leq t_j \leq t_e \\ \frac{R_M - R_m}{\bar{R}_I - \bar{R}_E} R_j + (R_m - \bar{R}_E) & \text{otherwise} \end{cases}, \quad (2)$$

where R denotes the ECG-derived respiration, $R_M = 6$ and $R_m = 3.5$ are the maximal and minimal breathing amplitudes [10], \bar{R}_I and \bar{R}_E are the mean values for the end of inspiration and expiration calculated from the data, and t_s and t_e are the start and end times of the VM extracted directly from the ITP data [35]. Heart rate is computed from the ECG signal using a built-in LabChart[®] function that detects RR intervals.

3.2. Model development

Taking SBP and P_{th} as inputs, the model predicts heart rate (H) as an output. Figure 3 displays a schematic of the model. The upper section, denoted with solid black arrows, represents the

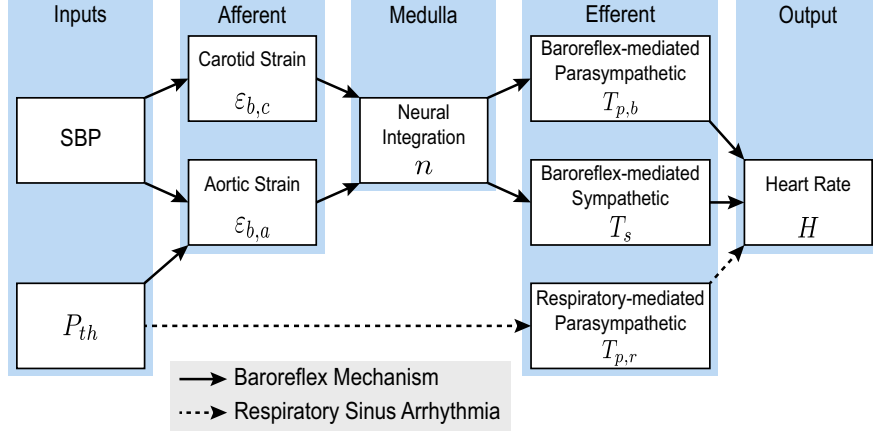


Figure 3: Model diagram reproduced from [35]. The model takes systolic blood pressure (SBP, mmHg, Figure 1c) and the thoracic pressure (P_{th} , mmHg, Figure 1d, equation (2)) as inputs. The baroreflex model (solid arrows) predicts the baroreceptor strains in the carotid sinus ($\varepsilon_{b,c}$, dimensionless, equation (5)) as a function of SBP and the aortic arch ($\varepsilon_{b,a}$, dimensionless, equation (5)) as a function of SBP and P_{th} . These signals are integrated in the medulla (n , s^{-1} , equation (6)). A signaling cascade initiates a dynamic change in baroreceptor-mediated parasympathetic ($T_{p,b}$, dimensionless, equation (8)) and sympathetic (T_s , dimensionless, equation (9)) pathways. The respiratory sinus arrhythmia model (dotted arrows) depends solely on P_{th} , as the thorax oscillates with normal breathing. Fluctuations in respiration modulate the respiratory-mediated parasympathetic outflow ($T_{p,r}$, dimensionless, equation (11)). All efferent outflows are combined to control the heart rate (H , bpm, equation (12)).

baroreflex pathway, and the lower section denoted with dotted black arrows encodes heart rate control via respiratory sinus arrhythmia (RSA).

The model assumes that the pressure in the carotid sinus is the same as the measured SBP and that the pressure in the aortic arch can be predicted from the SBP and P_{th} by

$$P_c = \text{SBP} \quad \text{and} \quad P_a = \text{SBP} - P_{th}. \quad (3)$$

The baroreceptors are embedded in the arterial wall, which deforms nonlinearly as arterial pressure increases [45]. Similarly to Mahdi et al. [25], we compute the strain of the arterial wall $\varepsilon_{w,j}$ for $j = c$ or a for carotid or aortic, respectively, as

$$\varepsilon_{w,j} = 1 - \sqrt{\frac{1 + e^{-q_w(P_j - s_w)}}{A + e^{-q_w(P_j - s_w)}}}, \quad (4)$$

where q_w (mmHg^{-1}) and s_w (mmHg) are the steepness and half-saturation value of the sigmoidal relationship and A (dimensionless) is an offset parameter. The strain of the baroreceptors as they deform along with the arterial wall is predicted using a linear ordinary differential equation (ODE) of the form

$$\frac{d\varepsilon_{b,j}}{dt} = \frac{-\varepsilon_{b,j} + K_b \varepsilon_{w,j}}{\tau_b}, \quad (5)$$

where K_b (dimensionless) and τ_b (s) are the gain and time-scale, respectively. The medulla receives signals from the baroreceptors, which sense the relative strain from rest [4]. We compute an integrated neural signal via a convex combination of the relative strains of both the aortic and carotid regions as

$$n = B(\varepsilon_{w,c} - \varepsilon_{b,c}) + (1 - B)(\varepsilon_{w,a} - \varepsilon_{b,a}), \quad B \in [0, 1]. \quad (6)$$

Note, if $B = 0$ (s^{-1}), the model depends solely on the aortic baroreceptors, and if $B = 1$, it depends solely on the carotid baroreceptors.

After the medulla receives signals from the baroreceptors, it inhibits the parasympathetic and stimulates the sympathetic nervous systems. To model these interactions, we use the sigmoidal functions

$$G_{p,b} = \frac{1}{1 + e^{-q_{p,b}(n-s_{p,b})}} \quad \text{and} \quad G_s = \frac{1}{1 + e^{q_s(n-s_s)}}, \quad (7)$$

where q_k (s) and s_k (s^{-1}) are the steepness and half-saturation values, respectively, for $k = p, b$ or s denoting baroreflex-mediated parasympathetic and sympathetic, respectively. The efferent signals, transmitted from the medulla to the heart, are the solutions to the differential equations

$$\frac{dT_{p,b}}{dt} = \frac{-T_{p,b} + K_{p,b}G_{p,b}}{\tau_{p,b}} \quad \text{and} \quad (8)$$

$$\frac{dT_s}{dt} = \frac{-T_s(t - D_s) + K_s G_s}{\tau_s}, \quad (9)$$

where K_k (dimensionless) and τ_k (s) are the gains and time-scale, respectively, and D_s (s) is the discrete delay in the sympathetic outflow. Figure 1e displays the time series for $T_{p,b}$ and T_s for this subject with optimized parameter values.

The respiratory-mediated parasympathetic outflow is modulated by the medulla as well. This signal has many inputs which are lumped into the thoracic pressure signal P_{th} . The integration of P_{th} into the medulla is determined by solving a decreasing sigmoid function

$$G_{p,r} = \frac{1}{1 + e^{q_{p,r}(P_{th}-s_{p,r})}}, \quad (10)$$

where $q_{p,r}$ (mmHg^{-1}) and $s_{p,r}$ (mmHg) are the steepness and half-saturation value. The efferent signal is modeled with the ODE

$$\frac{dT_{p,r}}{dt} = \frac{-T_{p,r} + K_{p,r}G_{p,r}}{\tau_{p,r}}, \quad (11)$$

where $K_{p,r}$ (dimensionless) and $\tau_{p,r}$ (s) denote the gain and time-scale.

Inspired by previous work [23, 31, 32], the heart rate is the solution to the ODE

$$\frac{dH}{dt} = \frac{-H + \tilde{H}}{\tau_H}, \quad (12)$$

where τ_H (s) is a time-scale and

$$\tilde{H} = H_I(1 - H_{p,b}T_{p,b} + H_{p,r}T_{p,r} + H_s T_s). \quad (13)$$

H_I (bpm) is the age-dependent intrinsic heart rate (when the sinoatrial node is denervated [15]), while $H_{p,b}$ (dimensionless), $H_{p,r}$ (dimensionless), and H_s (dimensionless) scaling parameters. Figure 1f shows the optimized model fit to the heart rate data.

In summary, heart rate is predicted as the solution to a system of stiff ODEs and DDEs of the form

$$\frac{d\mathbf{x}}{dt} = f(t, \mathbf{x}(t), \mathbf{x}(t - D_s); \theta), \quad \mathbf{x}(t) = \mathbf{x}_0 \text{ for } t \in [-D_s, 0], \quad (14)$$

where $\mathbf{x} = [\varepsilon_{b,c}, \varepsilon_{b,a}, T_{p,b}, T_{p,r}, T_s, H]^T \in \mathbb{R}^6$ is the vector of states, $f : \mathbb{R}^{1+2(6)+25} \rightarrow \mathbb{R}^6$ is the right hand side of the system, t denotes time in seconds, D_s (s) is the discrete delay, and $\theta \in \mathbb{R}^{25}$ is a vector of parameters, including

$$\theta = [A, B, K_b, K_{p,b}, K_{p,r}, K_s, \tau_b, \tau_{p,b}, \tau_{p,r}, \tau_s, \tau_H, q_w, q_{p,b}, q_{p,r}, q_s, s_w, s_{p,b}, s_{p,r}, s_s, H_I, H_{p,b}, H_{p,r}, H_s, t_s, t_e]^T. \quad (15)$$

Table 1 lists the nominal parameter values. Calculations of the initial conditions for the states are given in Appendix A. The model is solved using the Fortran implementation of the stiff DDE solver RADAR5 [9] with relative and absolute tolerances of 10^{-8} . The time-varying H model output was interpolated at the discretized time points from the heart rate data. As described in Appendix A, the model was fitted to the heart rate data by estimating a parameter subset that minimizes the least squares error between the model output and the data.

Upper and lower parameter bounds are given in Table 1. Parameters not calculated *a priori* are varied by $\pm 50\%$ of their nominal values. Parameters calculated from the data have bounds set to the mean value ± 2 standard deviations (SD). An exception is the parameter τ_s , which interacts with the delay D_s and can cause instability [36]. To remain in the stable region, τ_s is varied $\pm 50\%$ of its nominal value. The parameter B denoting the convex combination of aortic and carotid baroreceptors varies from 0 to 1. The GSA and the parameter estimation methods are performed on the logarithm of the parameters. Therefore, we enforce positivity by setting the lower bounds that became negative to 0.01.

3.3. Global sensitivity analysis

We use variance-based SIs [37, 41] for the GSA. This section discusses four different methods for computing SIs: scalar [37], pointwise-in-time [2], generalized [1], and limited-memory (new). A reference table of symbols is compiled in Table 2.

3.3.1. Scalar Sobol' indices

Consider a mathematical model f with a scalar output y dependent on $\theta \in \Omega_p \subseteq \mathbb{R}^p$, a vector of p uncertain model parameters with a prescribed parameter space Ω_p ; that is,

$$y = f(\theta). \quad (16)$$

For each parameter θ_i , we compute its contribution to the variance of y [40, 41]. Assuming that the parameters are independent, the main effect on f by varying θ_i is given by

$$S_i(f) = \frac{\mathbb{V}_{\theta_i}(\mathbb{E}_{\theta_{\sim i}}[f|\theta_i])}{\mathbb{V}(f)}, \quad (17)$$

where $\mathbb{V}(\cdot)$ and $\mathbb{E}[\cdot]$ denote the variance and expectation operators and $\theta_{\sim i}$ is the vector θ without parameter θ_i , that is

$$\theta_{\sim i} = [\theta_1, \theta_2, \dots, \theta_{i-1}, \theta_{i+1}, \dots, \theta_p]^T. \quad (18)$$

The total-effect scalar SI on f includes both the main and higher order effects of θ_i and is given by

$$\mathcal{T}_i(f) = \frac{\mathbb{E}_{\theta_{\sim i}}[\mathbb{V}_{\theta_i}(f|\theta_{\sim i})]}{\mathbb{V}(f)} = 1 - \frac{\mathbb{V}_{\theta_{\sim i}}(\mathbb{E}_{\theta_i}[f|\theta_{\sim i}])}{\mathbb{V}(f)}. \quad (19)$$

Table 1: Parameters.

Parameter Description and Symbol	Units	Nom value	Physiological Range (Mean \pm SD)	Lower bound	Upper bound	Bound Explanation
Offset						
A		5		2.5	7.5	Nom \pm 50%
Convex parameter						
B	s^{-1}	0.5		0.01	1	[0, 1]
Gains						
K_b		0.1		0.05	0.15	Nom \pm 50%
$K_{p,b}$		5		2.5	7.5	Nom \pm 50%
$K_{p,r}$		1		0.5	1.5	Nom \pm 50%
K_s		5		2.5	7.5	Nom \pm 50%
Time-scales						
τ_b	s	0.9		0.45	1.8	Nom \pm 50%
$\tau_{p,b}$	s	1.8	$6.5 \pm 5.7^*$	0.01	17.9	Mean \pm 2SD
$\tau_{p,r}$	s	6	$9.6 \pm 10.8^*$	0.01	31.2	Mean \pm 2SD
τ_s	s	10	$14 \pm 8^*$	5	15	Nom \pm 50%
τ_H	s	0.5		0.25	0.75	Nom \pm 50%
Sigmoid						
Steepnesses						
q_w	mmHg^{-1}	0.04		0.02	0.06	Nom \pm 50%
$q_{p,b}$	s	10		5	15	Nom \pm 50%
$q_{p,r}$	mmHg^{-1}	1		0.5	1.5	Nom \pm 50%
q_s	s	10		5	15	Nom \pm 50%
Half-saturation Values						
s_w	mmHg		$123 \pm 20^{**}$	83	163	Mean \pm 2SD
$s_{p,b}$	s^{-1}		$0.54 \pm 0.005^{**}$	0.53	0.55	Mean \pm 2SD
$s_{p,r}$	mmHg		$4.88 \pm 0.21^{**}$	4.46	5.3	Mean \pm 2SD
s_s	s^{-1}		$0.05 \pm 0.005^{**}$	0.04	0.06	Mean \pm 2SD
Heart rate Gains						
H_I	bpm		$100 \pm 7^{**}$	86	114	Mean \pm 2SD
$H_{p,b}$			$0.5 \pm 0.2^*$	0.1	0.9	Mean \pm 2SD
$H_{p,r}$			$0.3 \pm 0.4^*$	0.01	1.1	Mean \pm 2SD
H_s			$0.3 \pm 0.4^*$	0.01	1.1	Mean \pm 2SD
Delay						
D_s	s	3				
VM start/end						
t_s	s	data				
t_e	s	data				

Nom: nominal. SD: standard deviation. VM: Valsalva maneuver. Absence of units denotes dimensionless parameter. * denotes parameter range is from optimized parameter values from [35]. ** denotes values calculated from data.

Table 2: Summary of Sobol' index (SI) symbols.

SI Type	Symbol		Reference
	Main	Total	
Scalar	$\mathcal{S}_i(f)$	$\mathcal{T}_i(f)$	[37]
Time-varying			
Pointwise-in-time (PTSI)	$\mathcal{S}_i(f; t)$	$\mathcal{T}_i(f; t)$	[2]
Generalized (GSIs)	$\mathcal{S}_i(f; I_0^t)$	$\mathcal{T}_i(f; I_0^t)$	[1]
Limited-memory (LMSIs)	$\mathcal{S}_i(f; I_\Delta(t))$	$\mathcal{T}_i(f; I_\Delta(t))$	This study

$i = 1, \dots, p$ denotes the parameter index

$I_0^t = [0, t]$ and $I_\Delta(t) = [t - \Delta, t]$ for integration window Δ .

3.3.2. Time-varying Sobol' indices

The following formulations attempt to account for changes in parameter influence over time.

Pointwise-in-time Sobol' indices (PTSIs): Consider a model f with time-varying output $y(t)$ on an interval $I_T = [0, T]$ for end time point $T > 0$, i.e.,

$$y(t) = f(t; \theta), \quad t \in I_T. \quad (20)$$

For this model, the main effect PTSI of f by varying θ_i at time t is given by

$$\mathcal{S}_i(f; t) = \frac{\mathbb{V}_{\theta_i}(\mathbb{E}_{\theta_{\sim i}}[f(t; \cdot) | \theta_i])}{\mathbb{V}(f(t; \cdot))}, \quad t \in I_T, \quad (21)$$

and the total effect PTSI of f by varying θ_i at time t is given by

$$\mathcal{T}_i(f; t) = \frac{\mathbb{E}_{\theta_{\sim i}}[\mathbb{V}_{\theta_i}(f(t; \cdot) | \theta_{\sim i})]}{\mathbb{V}(f(t; \cdot))}, \quad t \in I_T. \quad (22)$$

Generalized Sobol' indices (GSIs): The indices in equations (21) and (22) ignore time correlations and the history of the time-dependent signal. The method proposed by Alexanderian et al. [1] takes into account time correlations by integrating the numerators and denominators of equations (21) and (22) over time. Let $I_0^t = [0, t]$ be a time-varying interval. The the main effect GSI of f by varying θ_i over the interval I_0^t is given by

$$\mathcal{S}_i(f; I_0^t) = \frac{\int_0^t \mathbb{V}_{\theta_i}(\mathbb{E}_{\theta_{\sim i}}[f(\tau; \cdot) | \theta_i]) \, d\tau}{\int_0^t \mathbb{V}(f(\tau; \cdot)) \, d\tau}, \quad t \in I_T. \quad (23)$$

Similarly, the total effect GSI on f by varying θ_i over the interval I_0^t is given by

$$\mathcal{T}_i(f; I_0^t) = \frac{\int_0^t \mathbb{E}_{\theta_{\sim i}}[\mathbb{V}_{\theta_i}(f(\tau; \cdot) | \theta_{\sim i})] \, d\tau}{\int_0^t \mathbb{V}(f(\tau; \cdot)) \, d\tau}, \quad t \in I_T. \quad (24)$$

The integrals in equations (23) and (24) are computed following the method in Appendix B.

Limited-memory Sobol' indices (LMSIs): By integrating over I_0^t , equations (23) and (24) compute the parameter influence up to time t , which can be interpreted as an average across I_0^t . However, this method might miss the contribution of the parameters during fast, transient

disturbances, especially for problems where an extended baseline is necessary to obtain steady-state conditions. To remedy this, we propose a new technique, *limited-memory* Sobol' indices, to analyze parameter influence as the QoI responds to transient disturbances in its steady-state behavior. To do so, we introduce a moving integration window $I_\Delta(t)$ of width Δ . The shape of the window and magnitude of Δ is necessarily problem-dependent. By implementing this window, the integration interval I_T necessarily decreases by Δ ; that is, the new integration interval is $I_{T-\Delta} = [\Delta, T]$. The main effect LMSI on f by varying θ_i over the interval $I_\Delta(t)$ is given by

$$\mathcal{S}_i(f; I_\Delta(t)) = \frac{\int_{t-\Delta}^t \mathbb{V}_{\theta_i}(\mathbb{E}_{\theta_{\sim i}}[f(\tau; \cdot) | \theta_i]) w(\tau) d\tau}{\int_{t-\Delta}^t \mathbb{V}(f(\tau; \cdot)) w(\tau) d\tau}, \quad t \in I_{T-\Delta}, \quad (25)$$

where $w(t)$ denotes the weights at each time point t_j determined by the window of choice. Similarly, the total effect LMSI on f by varying θ_i over the interval $I_\Delta(t)$ is given by

$$\mathcal{T}_i(f; I_\Delta(t)) = \frac{\int_{t-\Delta}^t \mathbb{E}_{\theta_{\sim i}}[\mathbb{V}_{\theta_i}(f(\tau; \cdot) | \theta_{\sim i})] w(\tau) d\tau}{\int_{t-\Delta}^t \mathbb{V}(f(\tau; \cdot)) w(\tau) d\tau}, \quad t \in I_{T-\Delta}. \quad (26)$$

By integrating the variances within a moving window, we can capture the transient changes in parameter influence (as in the PTSIs) but avoid missing short-lived responses (as in the GSIs).

There are many factors contributing to choosing the appropriate type, shape, and width of the window. In this study, we let the physiology guide window selection. Since both the blood pressure and the change in blood pressure affect the baroreflex modulation of heart rate, recent blood pressure and heart rate values contribute more to the current heart rate. Moreover, future time points have no bearing on the current heart rate. To accommodate these features, we used a Gaussian trailing window. Since the VM is typically 15 s in length, a window of about 15 s should suffice. We chose to use a trailing half-Gaussian integration window for $\Delta = 15$ s before time point t_j to coincide with the typical length of the VM. Further discussion of the moving window can be found in Section 5.3.

3.4. GSA Computation

The GSA was conducted using Monte Carlo integration including all model parameters ($p = 23$) except the Valsalva start and end times, t_s and t_e , which are extracted from the data. We computed $L_1 = 10^3(p + 2)$ resulting in 25,000 function evaluations [12, 22] and tested for convergence using $L_2 = 10^4(p + 2)$ with 250,000 function evaluations and $L_3 = 10^5(p + 2)$ with 2,500,000 function evaluations, which produced similar results. For the reduced models, we use L_1 evaluations, since the results did not change with larger sample sizes. To compute the variance and expectation given in equations (21)-(26), we used the method proposed by Saltelli et al. [37] (described in detail in Appendix B). To approximate the integrals in equations (23)-(26), we used the trapezoid quadrature scheme.

3.5. GSA-informed model reduction and selection

We compare the performance of each of the four methods discussed in Section 3.3. The scalar SIs are calculated with respect to the Euclidean norm of the residual \mathbf{r} , that is, $\mathcal{S}_i(\|\mathbf{r}\|_2)$ and $\mathcal{T}_i(\|\mathbf{r}\|_2)$, where \mathbf{r} is given in equation (1). Using $\|\mathbf{r}\|_2$ as the scalar model output gives a decent indication of

the sensitivity of \mathbf{r} to the parameters at steady-state, since the Euclidean norm can be considered an average of the signal over time. However, this disregards the changes in parameter influence as fast disturbances occur in the model output. Hence, in response to the time-varying \mathbf{r} , we simultaneously compute the PTSIs, GSIs, and LMSIs.

3.5.1. Sensitivity ranking

To identify parameters that do not influence the model output, we rank the total effect scalar SIs $\mathcal{T}_i(\|\mathbf{r}\|_2)$ and group them into three categories: most, moderately, and least influential. $\eta_1 = 10^{-1}$ is the threshold for moderately influential parameters assigned based on the clear separation in parameter influence values shown in Figure 4. $\eta_2 = 10^{-3}$ is assigned in accordance with the LSA conducted in our previous work [35]. The parameter groups designated by the scalar indices motivated the grouping used for the time-varying indices (PTSIs, GSIs, and LMSIs). We define a parameter θ_i as noninfluential over the time series if

$$\mathcal{T}_i(\mathbf{r}; t) < \eta_2 \quad \forall t \in I_T. \quad (27)$$

Parameters that satisfy this criterion will either be fixed at their nominal value or removed from the analysis by analytically excising the model component in which they appear.

3.5.2. Model reduction

Using the sensitivity ranking, we develop steps for an iterative model reduction methodology informed by the GSA. We use the results from the LMSIs to identify components of the model to remove. The steps are as follows:

1. Compute the time-varying indices \mathcal{T}_i for all parameters to be considered.
2. Determine if each \mathcal{T}_i satisfies the criterion in equation (27) for all time points. If so, this set of noninfluential parameters, θ_{NI} , is flagged for removal.
3. Analyze the parameters in θ_{NI} and determine if it is possible to remove the equations associated with each parameter. This step is problem-specific and inherently changes the mathematical structure of the model. Choose a parameter θ_k that has the least influence. Remove the components of the model associated with that parameter and restructure the model. We would like to stress that this is an iterative and model-specific process, as there are many instances where removing model components can be detrimental. Some changes to the model equations must occur simultaneously, which we will exemplify in the next section.
4. Recalibrate parameters to obtain new parameter vector θ^* for newly generated model f^* and run the model. f^* joins the set of models, \mathcal{M} .
5. Repeat GSA and then steps 2-4 on f^* . Iterate until the parameters in θ_{NI} are not algebraically removable. Fix all remaining parameters in θ_{NI} at their nominal values.

This process generates a set of models $\mathcal{M} = \{m_0, m_1, \dots, m_M\}$ for m_0 the full model and M the number of m_i reduced models.

3.5.3. Model selection

To compare model performance between the full and reduced models, we use a statistical measure that calculates a trade off between how well the model fits the data (goodness of fit) with how complex the model is (number of estimated parameters) [34]. To quantify this comparison, we use the AICc and BIC to calculate a regression between the model output and the data [47]. We assume that the residual errors are independent and identically distributed with mean zero and

finite variance. By predicting the maximum likelihood estimate, which is equivalent to minimizing the least squares error J (equation (A.9)), we compute

$$\text{AICc} = N \log \left(\frac{J}{N} \right) + 2(\hat{p} + 2) \left(\frac{N}{N - (\hat{p} + 2) - 1} \right) \quad \text{and} \quad (28)$$

$$\text{BIC} = N \log \left(\frac{J}{N} \right) + (\hat{p} + 2) \log(N), \quad (29)$$

where N is the number of data points and \hat{p} the length of the optimized parameter subset vector $\hat{\theta}$ [5]. To compare the models, we report the relative index of each model from the minimal model, that is

$$\text{AICc}_{rel} = e^{(\text{AICc}_{min} - \text{AICc}_i)/2} \quad \text{and} \quad (30)$$

$$\text{BIC}_{rel} = e^{(\text{BIC}_{min} - \text{BIC}_i)/2}. \quad (31)$$

This statistical technique is useful when determining the goodness of fit to data. However, there are other predicted model outputs, such as $T_{p,b}$ and T_s , that are of clinical importance since they cannot be measured without costly and invasive procedures that blunt the signals with anesthetization. Therefore, we must also assess the model performance qualitatively. We do so by comparing the reduced model to the full model predictions, assuming that the full model produces the true signal. Since the traces for $T_{p,b}$ are very similar, we employ the metric

$$Q = |\max(T_{s,m_0}) - \max(T_{s,m_i})| \quad (32)$$

determining the reduced model that minimizes the distance between the maxima of their respective T_s predictions.

In summary, these metrics account for both the model fits to data and the predicted quantities for which there is no data. Both aspects are crucial for an effective reduced model. The data and run-time environment for the model code can be found at DOI: 10.5281/zenodo.3856447.

4. Results

This section discusses the outcomes from the scalar Sobol' indices (SIs) (Figure 4) and the time-varying SIs: pointwise-in-time (PTSIs), generalized (GSIs), and limited-memory (LMSIs) (Figure 6). The latter is computed using a moving integration window of width Δ . We also compare several window widths (Figure 8). Using outcomes from the LMSIs, we inform a model reduction. Lastly, we select the best model by computing the relative Akaike Information Criterion with correction (AICc_{rel} , equation (30)) and relative Bayesian Information Criterion (BIC_{rel} , equation (31)) in Table 5 and by examining the predicted model outputs $T_{p,b}$ and T_s to give physiological predictions (Figure 7).

4.1. Sobol' indices

The scalar SIs are shown in Figure 4 and the time-varying SIs are shown in Figure 6. For each analysis, the parameters are divided into three influence groups: most ($> \eta_1$), moderately (between η_1 and η_2), and least ($< \eta_2$) influential.

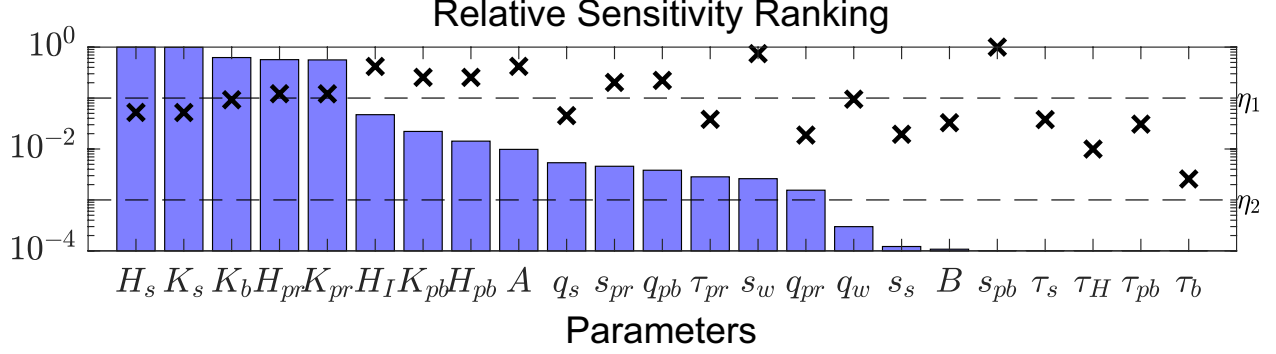


Figure 4: Relative scalar sensitivity analysis ranking with respect to $\|\mathbf{r}\|_2$. Influence thresholds $\eta_1 = 10^{-1}$ and $\eta_2 = 10^{-3}$ are indicated with horizontal dashed lines. Global sensitivity analysis results (blue bars) are computed using the scalar total effect Sobol' indices ($\mathcal{J}_i(\|\mathbf{r}\|_2)$) given in equation (19), scaled by the maximum sensitivity value and plotted on a logarithmic scale for the y -axis. Local sensitivity analysis results (black x's) are reproduced from [35].

4.1.1. Scalar Sobol' indices

Figure 4 shows the ranking of the total effect scalar SIs, ranked with respect to the Euclidean norm of the model output residual $\|\mathbf{r}\|_2$, that is, $\mathcal{J}_i(\|\mathbf{r}\|_2)$. These are plotted with the local sensitivity analysis (LSA) results reproduced from Randall et al. [35]. The five most influential parameters, i.e., $\{H_s, K_s, K_b, H_{p,r}, K_{p,r}\} > \eta_1$, are associated with RSA and the sympathetic tone during and after the VM. These parameters influence the controllers of heart rate both at rest (during the baseline) and during the transient impact of the VM. In comparison, the LSA determined that the parameters $s_{p,b}$, s_w , A , H_I were the most influential. Note that the LSA is evaluated at particular instant within the parameter space Ω_p and each of the parameters is changed one at a time, which could lead to a different parameter ranking.

The subset of least influential parameters, i.e., $\mathcal{J}_i(\|\mathbf{r}\|_2) < \eta_2$, is

$$\theta_{NI,sca} = \{q_w, s_s, B, s_{p,b}, \tau_s, \tau_H, \tau_{p,b}, \tau_b\}. \quad (33)$$

Figure 5 displaying 10 samples from the least sensitive parameters varied between their upper and lower bounds (given in Table 1) provides useful insight into how each parameter affects the output. Parameters s_s , $s_{p,b}$, τ_H , and τ_b have the least effect on the model output. The small effect of changing parameters s_s and $s_{p,b}$ is most likely due to their narrow distributions. In Randall et al. [35], these parameters are calculated *a priori* and do not vary much among the subjects studied. Parameters τ_H and τ_b have the least effect on the residual across all analyses.

4.1.2. Pointwise-in-time Sobol' indices

Figure 6 shows results for the most (Figure 6a), moderately (Figure 6d), and least (Figure 6g) influential parameters for the PTSIs. In the calculation of the PTSIs, the relative importance of each parameter is determined with respect to each time point. Comparisons between parameter influence measures at different time points can be difficult to interpret within one influence trace. The total effect SIs ($\mathcal{J}_i(\mathbf{r}; t)$) display rapid fluctuations. Since our goal is to determine regions where the influence of certain parameters increase or decrease substantially, the highly oscillatory nature of these solutions makes it difficult to compare the effect of each parameter, especially for the the least influential parameters.

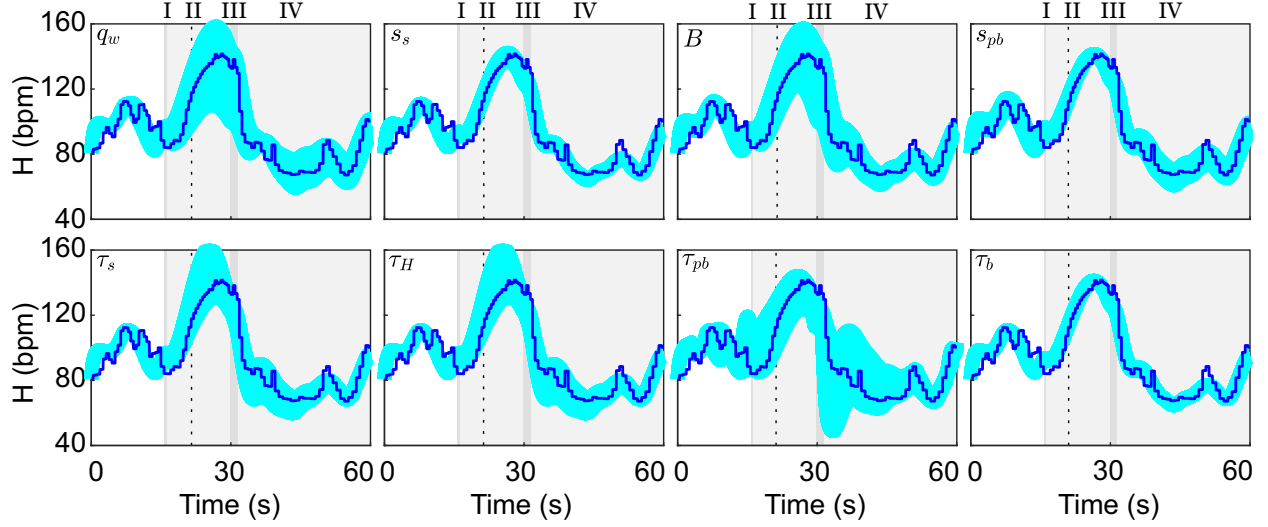


Figure 5: Noninfluential parameters as determined by the total effect scalar Sobol’ indices in Figure 4. The model was evaluated within the physiological range of each parameter given in Table 1 (cyan) plotted with the heart rate data (blue). The VM phases are represented as alternating gray (I and III) and light gray (II and IV) boxes. Phase II is divided into early and late parts (vertical dotted black line).

The most influential parameters are H_s , K_s , K_b , $H_{p,r}$, and $K_{p,r}$ (Figure 6a). Our results show that the sensitivity for K_b does not change significantly during the time interval, which is expected since the baroreceptors are always active. Parameters K_s and H_s are most influential, due to the activation of the sympathetic response after the onset of the VM. Finally, $H_{p,r}$ and $K_{p,r}$ decrease in influence below η_1 after the onset of the VM, due to parasympathetic withdrawal that occurs in phase II of the VM.

Parameters that remain under the threshold η_2 at all time include s_s , $s_{p,b}$, and τ_b . The half-saturation values are most likely small due to their narrow parameter distributions. It is surprising, though, that τ_b remains below η_2 , since all the other time-scales rise above η_2 at least one time point. These insensitive parameters are prime candidates for removal via the methods discussed in Section 3.

The pointwise-in-time technique designates almost all parameters as at least moderately influential at one point in time, which coincides with the results from the LSA. The oscillatory nature of the results complicates the determination of parameter influence level at different regions in the time series [1]. The PTSIs show that some of the parameters in $\theta_{NI,sca}$ become moderately influential over the time series, namely q_w , B , τ_s , τ_H , and $\tau_{p,b}$. However, these results do not provide much additional information that is not already given in both the scalar SI analysis and the LSA.

4.1.3. Generalized Sobol’ indices

As shown in Figures 6b, e, and h, the differences between the PTSIs and GSIs are evident. The former provides one case where the parameter influence oscillates significantly both at rest and during dynamic changes. It does not take into account the history of the variance, and even the baseline results are difficult to interpret. The latter places too much emphasis on the time-dependence, and hence, averages the signal over extended periods of baseline activity, missing any of the potential transient changes in parameter influence on the model output. These methods provide extremes for the analysis of these time-varying signals, as shown in Figure 8b where an example PTISI is in blue and GSI in red. These results suggest that there is a need for a method that

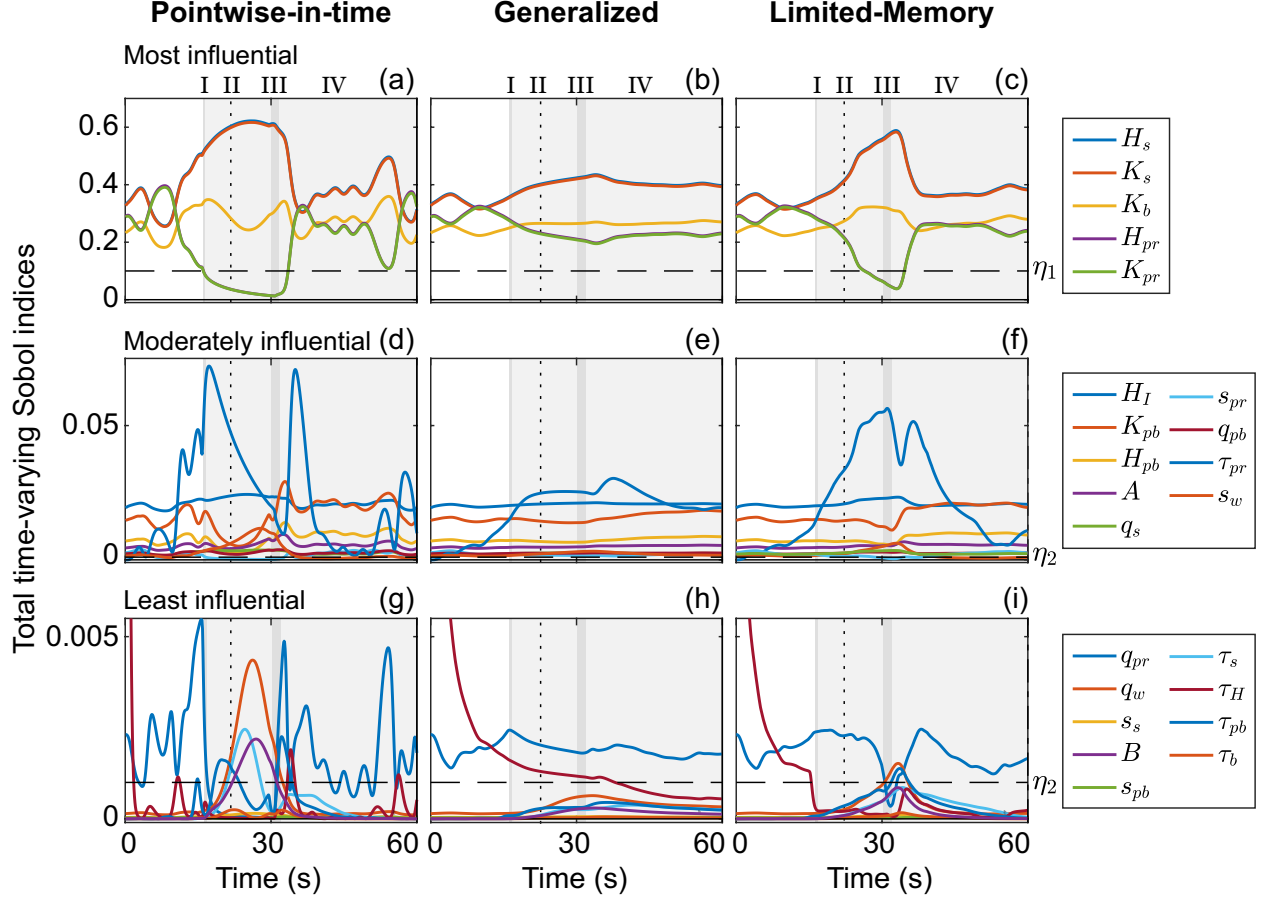


Figure 6: Time-varying total effect Sobol' indices (SIs) for the most (top row), moderately (middle row), and least (bottom row) influential parameters as determined by the scalar SIs in Figure 4 for the pointwise-in-time (a, d, g), generalized (b, e, h), and limited-memory (c, f, i) SIs. Thresholds $\eta_1 = 10^{-1}$ and $\eta_2 = 10^{-3}$ are indicated with horizontal dashed black lines. The VM phases are represented as alternating gray (I and III) and light gray (II and IV) boxes. Phase II is divided into early and late parts (vertical dotted black line).

incorporates both the transient nature of the PTSIs and the smoothing capabilities of the GSIs. As shown in Figure 6h, the least influential subset of parameters determined by the GSIs such that $\mathcal{T}(\mathbf{r}; I_0^t) < \eta_2$ for all time t is

$$\theta_{NI,G} = \{q_w, s_s, B, s_{p,b}, \tau_s, \tau_{p,b}, \tau_b\}. \quad (34)$$

Parameters $\tau_{p,r}$ (Figure 6e) and τ_H (Figure 6h) are notable exceptions to parameters with relatively constant traces. $\tau_{p,r}$ clearly increases in influence after the onset of the VM, which is to be expected as the influence of RSA decreases substantially during the VM. The time-scale for heart rate, τ_H , is moderately influential at the beginning of the time series but decreases in influence after the onset of the VM. This is surprising and may imply that τ_H plays an important role in establishing steady-state behavior from the initial conditions and then decreases in influence once steady-state is achieved.

4.1.4. Limited-memory Sobol' indices

Fluctuations in parameter influence correspond to different control mechanisms that activate and deactivate during the VM. We expect to observe the change in importance of parameters associated

Table 3: Noninfluential parameters from Sobol’ index methods.

Parameter	Sobol’ indices		
	Scalar	Generalized	Limited-memory
	$\theta_{NI,sca}$ (33)	$\theta_{NI,G}$ (34)	$\theta_{NI,LM}$ (35)
$q_{p,r}$	✓		
q_w	✓	✓	
s_s	✓	✓	✓
B	✓	✓	✓
$s_{p,b}$	✓	✓	✓
τ_s	✓	✓	✓
τ_H	✓		
$\tau_{p,b}$	✓	✓	
τ_b	✓	✓	✓

with activated control mechanisms that affect the heart rate dynamically. As shown in Figures 6c, f, and i, the LMSIs remain relatively constant before the VM. The LMSIs plotted in the figure have a trailing half-Gaussian moving window with $\Delta = 15$ s. It is important to choose a window that is short enough such that it can retain important features in the signal but long enough to be easily interpretable. Since the VM typically lasts 15 s, we compare the output from several window widths for $\Delta = 5, 10, 15$, and 20 s (Figure 8d). For smaller values of Δ , the LMSI converges to the PTSI, i.e., as $\Delta \rightarrow 0$, $\mathcal{S}(f; I_\Delta(t)) \rightarrow \mathcal{S}_i(t)$. For larger values of Δ , the LMSI converges to the GSI, i.e., as $\Delta \rightarrow T$, $\mathcal{S}_i(f; I_\Delta(t)) \rightarrow \mathcal{S}_i(f; I_0^t)$. Excluding $\Delta = 5$ and 20, the traces for $\Delta = 10$ and 15 are similar. To remain consistent with the VM itself, we chose a window of 15 s.

The LMSIs provide a balance between the PTSIs and GSIs by smoothing out the highly oscillatory PTSIs and incorporating the time-correlation structure preserved by the GSIs, if only for a small window of time. The LMSIs retain some modulation due to the transient nature of the VM, providing distinct changes in parameter influence rankings before, during, and after the VM. Therefore, we conclude that if the QoI is operating in steady-state, computing the scalar SIs would suffice for the analysis. However, during a transient disturbance from baseline, LMSIs provide a more informative parameter ranking.

The LMSIs show clear changes in parameter influence as time evolves. In particular, we observe increases in influence of parameters associated with T_s during the VM that subsequently decrease towards the end of phase IV. This behavior coincides with the activation of sympathetic tone during the VM and then deactivation after the release of the breath hold.

For the least influential parameters, $q_{p,r}$, q_w , τ_H , and $\tau_{p,b}$ become moderately influential within the interval I_T , while the subset

$$\theta_{NI,LM} = \{s_s, B, s_{p,b}, \tau_s, \tau_b\} \quad (35)$$

remains below η_2 . The half-saturation values $s_{p,b}$ and s_s are also in this subset due to their narrow distribution. τ_b has consistently been the least influential throughout all of the analyses and is expected to be in this subset. It is surprising that B and τ_s remain below η_2 for all t , since B determines the contribution of the aortic versus carotid baroreceptors. The necessity of this parameter has been supported in previous studies [20, 35], but the aim of the model reduction in the next section explores whether it is structurally necessary to include both baroreceptor regions. The sympathetic time-scale τ_s has been found in our previous work to be nonlinearly related to the delay D_s [36]. In this study, we have held D_s constant at 3 s and have only varied τ_s within parameter bounds that maintain stable model behavior (Table 1). Though our previous work shows the importance of τ_s , it may not be as influential to the heart rate residual in this range at $D_s = 3$.

In summary, the scalar SIs provide a clear parameter influence ranking that is similar to the ranking produced by the LSA. The time-varying techniques elucidate when a particular parameter

Table 4: Estimated parameter values.

Symbol	Model			
	m_0	m_1	m_2	m_3
B	0.43	0.58	0^\dagger	1^\dagger
$\tau_{p,b}$	4.27	4.05	3.85	4.62
$\tau_{p,r}$	2.71	2.61	2.68	2.58
$H_{p,b}$	0.43	0.43	0.42	0.43
$H_{p,r}$	0.48	0.46	0.50	0.39
H_s	0.28	0.32	0.20	0.47

[†]The B parameter was held constant at this value and not included as a part of the subset.

becomes important. Our results show that the GSIs have a clear benefit over the PTSIs, as they incorporate the time correlation structure of the signal. However, GSIs miss the effects of transient disturbances to steady-state behavior. Hence, we conclude that the LMSIs proposed in this study illustrate parameter influence traces that correspond to the modeled physiological phenomena. Table 3 summarizes the subsets of least parameters from the scalar SIs (equation (33)), GSIs (equation (34)), and LMSIs (equation (35)). The PTSIs were not included as their results were inconclusive. The LMSIs determined the smallest subset of noninfluential parameters for the entire time interval with 5, which are considered for removal in the model reduction in Section 4.2.

4.2. Model reduction

As stated in the protocol given in the Methods section (Section 3), we can “remove” parameters from consideration in two ways: (i) fix the parameter at its nominal value and rerun the analysis or (ii) analytically excise equations associated with the parameter in this subset. We first consider the parameters in this subset that we will fix at their nominal values based on the model structure. Secondly, we remove equations associated with noninfluential parameters and develop a suite of models upon which we can perform statistics.

4.2.1. Fixed parameters

Parameters $s_{p,b}$ and s_s are the half-saturation values appearing in equation (7). Their nominal values are computed *a priori* based on the assumption that 80% of the baseline heart rate is controlled by the baroreflex-mediated parasympathetic tone and 20% the baroreflex-mediated sympathetic tone [19, 35]. The coefficient of variation (SD/mean) for $s_{p,b}$ is 0.1%, which implies a very narrow dispersion.

As shown in our previous work [36], τ_s , appearing in equation (9), is nonlinearly related to the delay D_s and this relationship can lead to instability. Therefore, we restricted the upper and lower bounds of τ_s in this study to $\pm 50\%$ rather than use the entire physiological range (mean ± 2 SD) determined in [35] to ensure the parameter space Ω_p did not intersect an oscillatory regime. Therefore, we choose to fix τ_s at its nominal value.

After fixing these three parameters, we rerun the GSA calculating LMSIs. This analysis produced a similar plot to Figure 6i and τ_b and B are still in $\theta_{NI,LM}$ (results not shown). These results were computed with 25,000 samples, mimicking the strategy used with the original model. Since holding these parameters fixed produced very similar results, we will consider this analogous to the original model and refer to it as model m_0 .

4.2.2. Removed equations

From $\theta_{NI,LM}$, the time-scale for the baroreceptor strain τ_b and the convex combination parameter B are flagged for removal by changing the equations associated with these parameters.

Removing τ_b : The parameter τ_b appears in equation (5), the baroreceptor strains for the carotid and aortic baroreceptors. Since this value can be small and not impact the result, we can rearrange equation (5) as

$$\frac{d\varepsilon_{b,j}}{dt} = \frac{-\varepsilon_{b,j} + K_b\varepsilon_{w,j}}{\tau_b} \Rightarrow \tau_b \frac{d\varepsilon_{b,j}}{dt} + \varepsilon_{b,j} = K_b\varepsilon_{w,j}. \quad (36)$$

By letting $\tau_b = 0$, equation (5) is replaced with the algebraic relation

$$\varepsilon_{b,j}^* = K_b\varepsilon_{w,j}. \quad (37)$$

From here on, we will let the asterisk denote the new equations of the reduced system determined by the removal of τ_b . With this substitution, we have reduced the number of ODEs by two. Substituting equation (37) into equation (6) gives

$$\begin{aligned} n &= B(\varepsilon_{w,c} - \varepsilon_{b,c}^*) + (1 - B)(\varepsilon_{w,a} - \varepsilon_{b,a}^*) \\ &= B(\varepsilon_{w,c} - K_b\varepsilon_{w,c}) + (1 - B)(\varepsilon_{w,a} - K_b\varepsilon_{w,a}) \\ &= (1 - K_b)(B\varepsilon_{w,c} + (1 - B)\varepsilon_{w,a}) \\ &= (1 - K_b)n^* \end{aligned} \quad (38)$$

and we define

$$n^* = B\varepsilon_{w,c} + (1 - B)\varepsilon_{w,a}. \quad (39)$$

By substituting equation (38) into equation (7), we obtain

$$G_{p,b}^* = \frac{1}{1 + e^{-q_{p,b}(n - s_{p,b})}} \quad (40)$$

$$= \frac{1}{1 + e^{-q_{p,b}((1 - K_b)n^* - s_{p,b})}} \quad (41)$$

$$= \frac{1}{1 + e^{-q_{p,b}^*(n^* - s_{p,b}^*)}}, \quad (42)$$

and we define new parameter values

$$q_{p,b}^* = q_{p,b}(1 - K_b) \quad \text{and} \quad (43)$$

$$s_{p,b}^* = n^* + \frac{1}{q_{p,b}^*} \ln \left(\frac{K_{p,b}}{\bar{T}_{p,b}} - 1 \right), \quad (44)$$

where $\bar{T}_{p,b}$ is the steady-state value. New parameters q_s^* and s_s^* are determined similarly. The new

system of equations without the baroreceptor strain differential equations is

$$\varepsilon_{w,j} = 1 - \sqrt{\frac{1 + e^{-q_w(\bar{P}_j - s_w)}}{A + e^{-q_w(\bar{P}_j - s_w)}}} \quad \text{for } j = c \text{ or } a, \quad (45)$$

$$n^* = B\varepsilon_{w,c} + (1 - B)\varepsilon_{w,a}, \quad (46)$$

$$\frac{dT_{p,b}}{dt} = \frac{1}{\tau_{p,b}}(-T_{p,b} + K_{p,b}G_{p,b}), \quad G_{p,b} = \frac{1}{1 + e^{-q_{p,b}^*(n^* - s_{p,b}^*)}} \quad (47)$$

$$\frac{dT_s}{dt} = \frac{1}{\tau_s}(-T_s(t - D_s) + K_s G_s), \quad G_s = \frac{1}{1 + e^{q_s^*(n^* - s_s^*)}} \quad (48)$$

$$\frac{dT_{p,r}}{dt} = \frac{1}{\tau_{p,r}}(-T_{p,r} + K_{p,r}G_{p,r}), \quad G_{p,r} = \frac{1}{1 + e^{-q_{p,r}(P_{th} - s_{p,r})}} \quad (49)$$

$$\frac{dH}{dt} = \frac{1}{\tau_H}(-H + \tilde{H}), \quad \tilde{H} = H_I(1 - H_{p,b}T_{p,b} + H_{p,r}T_{p,r} + H_s T_s). \quad (50)$$

This new system of ODEs and DDEs consists of 4 states and 23 parameters. Let \cdot^* denote the reduced system

$$\frac{d\mathbf{x}^*}{dt} = f^*(t, \mathbf{x}^*(t), \mathbf{x}^*(t - D_s); \theta^*), \quad (51)$$

where f^* is given by equations (45)–(50), $\mathbf{x}^* = [T_{p,b}, T_{p,r}, T_s, H]^T \in \mathbb{R}^4$, D_s is the delay, and

$$\theta^* = [A, B, K_{p,b}, K_{p,r}, K_s, \tau_{p,b}, \tau_{p,r}, \tau_s, \tau_H, q_w, q_{p,b}^*, q_{p,r}, q_s^*, s_w, s_{p,b}^*, s_{p,r}, s_s^*, H_I, H_{p,b}, H_{p,r}, H_s, t_s, t_e]^T \in \mathbb{R}^{23}. \quad (52)$$

We refer to this reduced model as m_1 .

To determine a subset of parameters to optimize for m_1 , we perform subset selection using the structured correlation analysis described in Appendix A and obtain

$$\hat{\theta}_{m_1} = [B, \tau_{p,b}, \tau_{p,r}, H_{p,b}, H_{p,r}, H_s]^T. \quad (53)$$

Table 4 summarizes the optimized parameters for m_0 and m_1 . We perform GSA on m_1 , holding parameters $s_{p,b}$, s_s , and τ_s fixed and observe that B is the only remaining parameter below η_2 for all time t (results not shown).

Removing B : The convex combination parameter B in equation (39) determines the relative contribution of the afferent signals from the aortic and carotid baroreceptors. The necessity of delineating these baroreceptor regions has been explored in two previous studies [20, 35] and it is surprising that this parameter has been flagged for removal using the protocol given in the Methods section (Section 3). It is unknown how the aortic and carotid signals are integrated in the medulla and not clear whether it is sufficient to model only one of these regions. From Figure 6i, we observe that the influence of B is close to zero, but as the VM progresses, B increases, corresponding to the stimulation of the baroreceptors. After the breath hold ends, B returns to zero. To remove the equation associated with B , we observe in equation (39) that B vanishes when it is zero, indicating that the aortic baroreceptor strain solely influences the efferent response, or one, indicating carotid effects. This produces the following models: m_2 where $B = 0$ and

$$n_2^* = \varepsilon_{w,a}, \quad (54)$$

producing a system of ODEs and DDEs with 4 states and 22 parameters

$$\frac{d\mathbf{x}_2^*}{dt} = f_2^*(t, \mathbf{x}_2^*(t), \mathbf{x}_2^*(t - D_s); \theta_2^*), \quad (55)$$

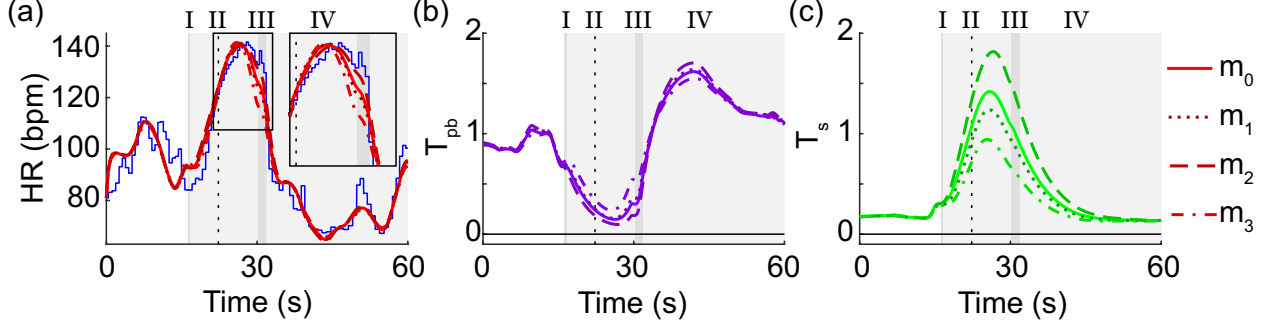


Figure 7: Plots of full (m_0 , solid) and reduced models. Reduced model 1 (m_1 , dotted) - removed 2 states and two parameters with parameter B estimated. Reduced model 2 (m_2 , dashed) - same as m_1 except with $B = 0$. Reduced model 3 (m_3 , dash-dotted) - same as m_1 except with $B = 1$. The Valsalva maneuver (VM) phases are represented as alternating gray (I and III) and light gray (II and IV) boxes. Phase II is divided into early and late parts (vertical dotted black line). (a) Model fits (red) to the heart rate data (blue). Insert shows a zoom of the heart rate fit in late phase II and phase III of the VM. (b) Model predictions of the efferent baroreflex-mediated parasympathetic ($T_{p,b}$, purple) for the full and reduced models. (c) Model predictions of the efferent baroreflex-mediated sympathetic (T_s , green) for the full and reduced models.

where f_2^* is the right hand side, $\mathbf{x}_2^* = [T_{p,b}, T_{p,r}, T_s, H]^T \in \mathbb{R}^4$ and

$$\theta_2^* = [A, K_{p,b}, K_{p,r}, K_s, \tau_{p,b}, \tau_{p,r}, \tau_s, \tau_H, q_w, q_{p,b}^*, q_{p,r}^*, q_s^*, s_w, s_{p,b}^*, s_{p,r}^*, s_s^*, H_I, H_{p,b}, H_{p,r}, H_s, t_s, t_e]^T \in \mathbb{R}^{22}; \quad (56)$$

and m_3 where $B = 1$ and

$$n_3^* = \varepsilon_{w,c} \quad (57)$$

producing a system of ODEs and DDEs with 4 states and 22 parameters

$$\frac{d\mathbf{x}_3^*}{dt} = f_3^*(t, \mathbf{x}_3^*(t), \mathbf{x}_3^*(t - D_s); \theta_3^*), \quad (58)$$

where f_3^* is the right hand side, $\mathbf{x}_3^* = \mathbf{x}_2^*$ and $\theta_3^* = \theta_2^*$. Using the structured correlation analysis method given in Appendix A, we obtain

$$\hat{\theta}_{m_2} = \hat{\theta}_{m_3} = [\tau_{p,b}, \tau_{p,r}, H_{p,b}, H_{p,r}, H_s]^T. \quad (59)$$

Table 4 lists the estimated parameters for models m_2 and m_3 . We perform GSA on each model, which results in all parameters above threshold η_2 at at least one time point within the interval I_T (results not shown). Hence, there are no parameters remaining in the noninfluential subset.

In summary, the model reduction methodology has produced 4 possible models, summarized in Table 4: m_0 where parameter $s_{p,b}$, s_s , and τ_s are held constant; m_1 where the equations associated with τ_b are removed; m_2 where τ_b is removed and $B = 0$; and m_3 where τ_b is removed and $B = 1$. Figure 7 plots each of the model fits to the data along with their respective $T_{p,b}$ and T_s traces.

4.3. Model selection

To determine which model best fit the data, we perform model selection protocol both quantitatively and qualitatively. The quantitative approach involves computing the relative AICc and BIC given in equations (30) and (31), respectively, assessing the model fit to the data, while the qualitative analysis investigates the importance for prediction of $T_{p,b}$ and T_s as they evolve in time. The latter

Table 5: Statistical analysis for model selection.

Model	Cost J (10^{-3}) (A.9)	Parameters p	Quantitative		Qualitative Q (32)
			$AICc_{rel}$ (30)	BIC_{rel} (31)	
m_0	4.64	6	0.83	0.83	
m_1	4.63	6	1	1	0.17
m_2	4.97	5	2.5e-4	3.6e-4	0.41
m_3	4.97	5	2.5e-5	3.6e-5	0.48

AICc - Akaike Information Criterion with correction in equation (28).

BIC - Bayesian Information Criterion in equation (29) .

is important, since the goal of our model is not only to fit the data but also to predict the neural tones that cannot be measured *in vivo* without blunting the parasympathetic and sympathetic responses with anesthetization. Hence, we test the reduced models by comparing the $T_{p,b}$ and T_s predictions to those obtained with the original model m_0 .

4.3.1. Goodness of fit analysis

We computed the relative AICc and BIC values, $AICc_{rel}$ and BIC_{rel} , respectively, for each of the models, assuming that the residuals are independent and identically distributed. From Table 5, we observe that m_1 has the greatest $AICc_{rel}$ and BIC_{rel} values. This is surprising, since m_1 estimates more model parameters than both m_2 and m_3 , which typically yield greater $AICc_{rel}$ and BIC_{rel} values [47]. Therefore, this analysis suggests that modeling both the aortic and carotid baroreceptor regions is necessary to predict heart rate.

4.3.2. Qualitative assessment

Figure 7 shows the H , $T_{p,b}$, and T_s traces for all of the models considered: m_0 (solid curve), m_1 (dotted curve), m_2 (dashed curve) and m_3 (dash-dotted curve). The model fits to heart rate data (Figure 7a) are all similar, which is expected since the model is calibrated to this representative data set. The least squares costs of the fits are of the same magnitude (Table 5). Interestingly, m_2 is the only model that is able to fit phase III of the data (Figure 7a insert), suggesting from a qualitative standpoint that m_2 captures the most features of the heart rate data. Figure 7b displays the predicted $T_{p,b}$ trace for the models, which are all similar and difficult to compare. However, Figure 7c shows the trajectories for T_s , exhibiting the greatest deviation from m_0 . Since traces for heart rate and $T_{p,b}$ for all four models are similar, we use T_s to compare the reduced models to the full model via the Q value (equation (32)). Table 5 compiles these metrics and m_1 has the lowest Q value. This result gives credence to the assertion that both the aortic and carotid baroreceptors must be included to predict heart rate and the neurological signals.

In summary, we conclude that m_1 , the reduced model after removing the equations associated with τ_b , is the best model for the biological questions investigated here. The $AICc_{rel}$ and BIC_{rel} values are the greatest while the qualitative metric Q was the lowest. This model predicts the heart rate the “best” with respect to complexity and number of parameters estimated, and the sympathetic output is closest to the original model.

5. Discussion

This study performs model reduction and selection using global sensitivity analysis (GSA) on a cardiovascular model predicting parasympathetic ($T_{p,b}$) and sympathetic (T_s) nervous outflow and heart rate (H) in response to the Valsalva maneuver (VM). For the GSA, we used Sobol’ indices (SIs), conducting our analysis with respect to a scalar quantity of interest (QoI), computed using

the Euclidean norm of the heart rate residual $\|\mathbf{r}\|_2$, and a time-varying QoI, the vector \mathbf{r} given in equation (1). Computation for the scalar SIs [37] was done with respect to $\|\mathbf{r}\|_2$ while the time-varying pointwise-in-time (PTSIs) [2], generalized (GSIs) [1], and limited-memory (LMSIs) Sobol' indices are with respect to \mathbf{r} . A novel component is the introduction of the LMSIs using a moving integration window Δ motivated by the transient VM process. The scalar SIs determined a ranking of parameter influence on the model output averaged over the entire time interval. We were able to categorize parameters based on their influence on the model output into three groups: most, moderately, and least influential. Additionally, the LMSIs informed a model reduction protocol that generated four models, m_0 , m_1 , m_2 , and m_3 . We analyzed the performance of these models qualitatively, comparing the model predicted signals to the original model m_0 , and quantitatively, calculating the relative Akaike Information Criterion with correction (AIC_{rel} , equation (30)) and the Bayesian Information Criterion (BIC_{rel} , equation (31)) for each model. m_1 proved to be the best model, implying the necessity of modeling both the aortic and carotid baroreceptor regions to predict heart rate accurately.

5.1. Local versus global sensitivity analysis

This study focused on the use of a GSA to analyze the sensitivity of the model output to the input parameters. These methods are computationally expensive, whereas a LSA method may suffice. In Randall et al. [35], we performed a LSA on the neural model presented here, reproduced in Figure 4. LSA is useful in its relative ease in computation, especially using approximations of derivatives with forward or central differences [17] and in its ability to calculate time-varying sensitivities. In steady-state with nominal parameters close to their optimal value, LSA is very useful in ranking parameter influence as shown in our previous work [7, 24, 27, 30]. The results from the LSA are similar to the ranking generated with scalar SIs, especially in regard to the least influential parameters τ_H and τ_b . Since every parameter in the LSA was above $\eta_2 = 10^{-3}$, every parameter is influential. However, this is just a snapshot of the model sensitivity at one instance in the parameter space. The benefit of GSA is that it explores the entire parameter space Ω_p and incorporates parameter interactions. Though there are some differences, the parameter rankings for both the LSA and GSA are similar, which could be due to the *a priori* calculation of nominal parameter values. Others have also found agreement in the calculation of the local and global parameter influences [22].

5.2. Time-varying GSA

In this study, we used SIs for the GSA. Though there are many other methods that explore the parameter space, including Morris screening [29] and derivative-based GSA methods [42], we use this approach due to its broad applications. We developed LMSIs including a moving window of width Δ , since the VM induces fast, transient changes in the steady-state behavior. Moving windows have been implemented in graphical sensitivity analysis, but this method has difficulty capturing the effects between parameters [14]. The LMSIs mitigate this issue by incorporating both parameter interactions and the history of the parameter variance. Another advantage of this approach is that it can be used for virtually any modeling effort analyzing parameter sensitivity over time.

Surely, not every problem requires time-varying GSA, and choosing to use this approach depends greatly on the questions asked and the QoI. Scalar SIs are appropriate if the QoI is a scalar, in steady-state, at a particular time point in the interval, or periodic with a constant frequency. However, if the objective is to understand parameter influence during a transition of states, this time-varying approach could provide rich information. One such study is that of Calvo et al. [6], which calculated SIs for the parameters of a cardiovascular model studying head-up tilt at rest and

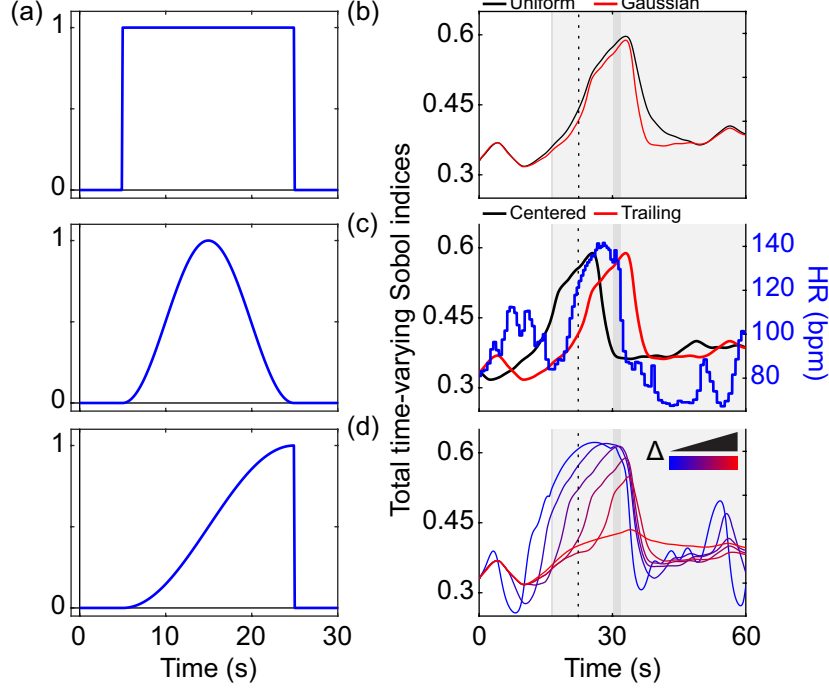


Figure 8: Moving window of integration, Δ , for a generic parameter θ_i . The Valsalva maneuver (VM) phases are represented as alternating gray (I and III) and light gray (II and IV) boxes. Phase II is divided into early and late parts (vertical dotted black line). (a) Common moving windows include uniform (top) for both centered and trailing windows, full Gaussian for centered windows, and half-Gaussian for trailing windows. (b) Comparison of uniform (black) versus (Gaussian) windows of width $\Delta = 15$ s. The Gaussian window shows a steeper decline in parameter influence in phase IV. (c) Comparison of centered (black) versus trailing (red) windows of width $\Delta = 15$ s overlaid the heart rate (HR, bpm) data (blue, right axis). The centered window shows an increase in parameter influence before the VM occurs. (d) Comparison of varying window lengths for increasing $\Delta = [5, 10, 15, 20]$ s. Pointwise-in-time Sobol' indices (blue) and generalized Sobol' indices (red) are also plotted.

during the tilt. The transition between these states as the tilt occurs is of great clinical interest, and hence, this study can benefit from using the LMSIs proposed here to measure the changes in parameter influence. Another is the study by Sumner et al. [44] that claims to analyze time-dependent parameter influence with SIs. However, the QoI for this model is the state predicting glycogen synthase kinase evaluated when $t = 60$, which is a scalar value, and only time-dependent in the sense that the QoI is a time point. If other time points are of interest, especially involving peaks of various compounds, either GSIs or LMSIs can be used to quantify the parameter influence over the entire time span up to 60 s.

5.3. Integration window

Moving windows have been used in signal processing for decades and relatively recently in graphical sensitivity analysis [14, 43]. A moving window, Δ , typically results in smoothing of the signal to determine mean behavior and enhance interpretability. However, there are several considerations when choosing an appropriate Δ for analysis of the biological problem: shape, type, and width. Shape refers to the functional form providing the weights for the window. Type refers to whether the window is calculated as trailing the current time point t_j or centered about t_j . Width refers to the time interval over which the window applies. We strongly suggest allowing the features of the system studied to dictate choice of window. In our study, much effort went into determining the most appropriate window for our problem.

Shape and type of window are interrelated, as choosing one can have bearing on the other. There are many potential window shapes, but here we discuss the most common types: uniform and Gaussian. Figure 8a displays uniform, half-Gaussian, and full Gaussian window. A uniform window will apply equal weight to each time point in the interval and, therefore, is independent of type of window. However, a Gaussian shape can be influenced by whether the window is trailing or centered. Choosing a half-Gaussian shape may be appropriate for trailing windows, placing more emphasis on the most recent time points, whereas a full Gaussian would be more applicable for a centered window. Figure 8b compares the traces from both a uniform (black) and a Gaussian (red) shape, though the differences are negligible. We allowed the physiology to dictate the appropriate window, so we chose a trailing window with the shape of a half-Gaussian, diminishing importance of the signal going further back in time. The half-Gaussian window defines a continuous function along the interval I_0^t , as the weights of the points outside the interval are zero. Figure 8c compares the results for trailing half-Gaussian and a centered full Gaussian overlaid the heart rate trace. Clearly, the centered window places the parameter influence before the VM occurs, showing a change in parameter influence before the change to the steady-state even begins. Since the trailing window coincides with the VM itself, especially the increase in parameter influence during late phase II, we chose to allow the window to trail t_j , as future time points do not impact the heart rate.

5.4. Model reduction

Due to the overall model complexity, understanding the biological implications of the results and parameter interactions can be difficult. Therefore, model reduction can simplify these interactions and still retain its predictive power. Many model reduction techniques exist from engineering and control theory [3], aiming to reduce large numbers of state variables with many nonlinearities by attempting to mitigate the same inherent problem we address here: to what extent do the input parameters affect the output. Our method using GSA to inform an analytical model reduction uses this idea to make appropriate choices for the exclusion of certain model components, unlike methods that solely approximate the input-output relationship without considering the other predicted model quantities [39]. To our knowledge, there are no previous studies that inform a model reduction based on time-varying GSA methods for physiological models. For biological systems with scalar QoIs, there has been a methodology proposed for model reduction via GSA by Marino et al. [26]; however, a statistical analysis of a group of reduced models was not conducted.

In this study, we have developed the LMSIs to specifically address this issue of substantial, transient disturbances in the steady-state behavior of the model and how the parameters impact the variance of the model output. An advantage of this approach is that it takes into account higher order parameter interactions and also the time correlation structure of the problem. Moreover, the implementation of the moving window increased the interpretability of the PTSIs, which are too oscillatory to decipher. Hence, the LMSIs can provide a clearer ranking while still retaining the transient fluctuations during the VM.

Though we acknowledge that SIs may be impractical for very large differential equation systems with hundreds of state variables and parameters, such as pharmacokinetics models, we suggest a multi-level approach. One can use simpler to compute but possibly less informative GSA measures first to identify a set of unimportant parameters and then perform a more comprehensive analysis on the remaining parameters [13]. We propose our GSA-informed model reduction methodology as an alternative approach to the balanced truncation method in the model reduction formulation proposed by Snowden et al. [39].

5.5. Model selection

To our knowledge, no previous studies have performed a model selection protocol for cardiovascular models in response to the VM. We employ relative AICc and BIC scores to compare the model fits to data. To consider the effect of reducing the full model on the other predicted quantities for which data is difficult to acquire, we combine quantitative and qualitative approaches to select whether the delineation between the baroreceptors of the carotid sinus and aortic arch is necessary to model, and, if not, which pathway should be modeled. We perform our analysis on our set of models $\mathcal{M} = \{m_0, m_1, m_2, m_3\}$ where m_0 is the original model with parameters $s_{p,b}$, s_s , and τ_s held fixed at their nominal values, m_1 is a reduced model of four states with τ_b removed, m_2 is the same as m_1 with convex combination parameter $B = 0$ emphasizing the aortic contribution only, and m_3 is the same as m_1 with $B = 1$ considering the carotid contribution only. The statistical analysis shows that m_1 fit the data best with the greatest relative AICc and BIC scores compared to the other models. This implies that it is necessary to model both the aortic and the carotid baroreceptor regions to predict heart rate. We compared each of the reduced models to m_0 via the metric Q given in equation (32), which measures the distance of the peak of T_{s,m_0} . m_1 has the lowest Q value is the closest to m_0 . Ultimately, we conclude that m_1 is the best model both to fit the heart data and predict the autonomic tones, and therefore, both regions are necessary to model the VM. Previous studies have modeled baroreceptor stimulation of only the carotid region [21, 23], though to our knowledge there are no studies solely modeling the aortic baroreceptors. Our previous work and the works of others [20, 35] support that modeling both regions is important and the analysis of the present study also agrees with this assertion.

5.6. Limitations

The GSA method of choice is highly dependent on the model formulation and the QoI. Choosing a computationally expensive GSA may not be feasible for models with long evaluation times, and the GSA results will differ based on the choice of QoI. For our choice of GSA, SIs assume that the model parameters are statistically independent and may not be reasonable for some models. Since model reduction was the focus of this study, we chose to take the analytical reduction approach, though we could have fixed τ_b at a constant value. Furthermore, analytical model reduction may also be impractical for very large systems with many parameters. In this case, setting the parameters to their nominal values may be more reasonable. Lastly, the results of the statistical analysis using AICc and BIC scores is highly dependent on the available data. If a different heart data set had been used, there is a possibility that the outcome of the model selection protocol could have been different. However, we conducted this analysis on three representative control subjects and achieved similar results as those produced in Section 4 (not shown).

6. Conclusions

In this study, we introduced a model reduction and selection process informed by global sensitivity analysis on a neurological model predicting heart rate and autonomic nervous function in response to the Valsalva maneuver. We have established a systematic framework for parameter dimension reduction and model simplification using global sensitivity analysis and developed the novel limited-memory Sobol' indices that are aware of time history as well as transient dynamics. Furthermore, we applied this methodology to a complex physiological model of the Valsalva maneuver response with extensive numerical experiments, simplifying the model while retaining important characteristics. From this methodology, we conclude that modeling both the aortic and carotid baroreceptor regions are necessary to achieve the appropriate dynamics of the Valsalva maneuver.

7. Acknowledgments

We would like to thank Dr. Pierre Gremaud for his help in the development and critical analysis of the limited-memory Sobol' indices.

8. Funding

This study was supported in part by the National Science Foundation under awards NSF/DMS 1246991 and NSF/DMS 1557761 and in part by the National Institute of Health HL139813.

Appendix A.

This appendix contains calculations of the initial conditions (ICs) of the system in equation (14) and details concerning the parameter subset selection methods.

Appendix A.1. Initial conditions

The ICs are computed to ensure the model is in steady-state by taking into account the baseline systolic blood pressure \bar{P} , thoracic pressure \bar{P}_{th} , and heart rate \bar{H} values, that is,

$$\bar{P}_c = \bar{P} \quad \text{and} \quad \bar{P}_a = \bar{P} - \bar{P}_{th}. \quad (\text{A.1})$$

From here on, $\bar{\cdot}$ denotes the steady-state condition. The ICs for the carotid ($\varepsilon_{b,c}$) and aortic ($\varepsilon_{b,a}$) baroreceptor strains (equation (5)) are computed as

$$\bar{\varepsilon}_j = K_b \bar{\varepsilon}_{w,j} = K_b \left(1 - \sqrt{\frac{1 + e^{-q_w(\bar{P}_j - s_w)}}{A + e^{-q_w(\bar{P}_j - s_w)}}} \right), \quad (\text{A.2})$$

where $j = c$ or a for carotid and aortic, respectively. The steady-state neural integration equation is the algebraic relation

$$\bar{n} = B(\bar{\varepsilon}_{w,c} - \bar{\varepsilon}_{b,c}) + (1 - B)(\bar{\varepsilon}_{w,a} - \bar{\varepsilon}_{b,a}). \quad (\text{A.3})$$

The efferent states have ICs $\bar{T}_{p,b} = 0.8$ and $\bar{T}_s = 0.2$ based on the assumption that 80% of baroreflex contribution to heart rate is due to the parasympathetic nervous system and 20% due to sympathetic [19]. We compute the IC for the respiratory-mediated parasympathetic tone as

$$\bar{T}_{p,r} = K_{p,r} \bar{G}_{p,r} = \frac{K_{p,r}}{1 + e^{-q_{p,r}(\bar{P}_{th} - s_{p,r})}}. \quad (\text{A.4})$$

The IC for the model output heart rate is \bar{H} .

Appendix A.2. Subset selection and parameter estimation

Motivated by our previous work [30, 33, 45], we determine a subset of parameters $\hat{\theta}$ to optimize using the structured correlation analysis approach. We compute the i^{th} column of a sensitivity matrix (\mathbf{S}) of the model residual \mathbf{r} with respect to the logarithm of the parameters (which vary in magnitude) at time t_j as

$$S_{ij} = \frac{\partial \mathbf{r}(t_j)}{\partial \log \theta_i} = \frac{\partial}{\partial \theta_i} \frac{H_m(t_j; \theta) - H_d(t_j)}{H_d(t_j)} \theta_i = \frac{\partial H_m(t_j; \theta)}{\partial \theta_i} \frac{\theta_i}{H_d(t_j)} \quad (\text{A.5})$$

for H_m the model output heart rate and H_d the observed data. This analysis is local in that the derivatives computed are evaluated at the nominal parameter values. To determine possible pairwise correlations between influential parameters as shown in our previous work [30], we calculate a correlation matrix \mathbf{c} from a covariance matrix

$$\mathbf{C} = (\tilde{\mathbf{S}}^T \tilde{\mathbf{S}})^{-1} \quad (\text{A.6})$$

as

$$c_{ij} = \frac{C_{ij}}{\sqrt{C_{ii}C_{jj}}}, \quad (\text{A.7})$$

where $\tilde{\mathbf{S}}$ are the columns of \mathbf{S} corresponding to the parameters in the subset $\hat{\theta}$. The matrix \mathbf{c} is symmetric with $|c_{ii}| = 1$ and $|c_{ij}| \leq 1$. For this study, we assigned a threshold of 0.9 for correlated parameters.

In the structured correlation analysis, we removed parameters from consideration *a priori*, such as the sigmoidal steepness parameters (q_i) and the half-saturation values (s_i). Optimizing these parameters can force the model to produce linear relations where nonlinearity occurs, producing results that are not physiological [35]. We also excluded the time parameters t_s and t_e from consideration as they were determined directly from the data and are naturally very influential to the model output.

Applying these methods to the given model produced the identifiable parameter subset

$$\hat{\theta} = [B, \tau_{p,b}, \tau_{p,r}, H_{p,b}, H_{p,r}, H_s]^T. \quad (\text{A.8})$$

More details can be found in [35]. We fit H to data by minimizing the least squares cost (J) between the model output and the data, i.e.,

$$J(\hat{\theta}) = \mathbf{r}^T \mathbf{r} + \left(\frac{\max_j H_m(t_j; \theta) - \max_j H_d(t_j)}{\max_j H_d(t_j)} \right)^2, \quad (\text{A.9})$$

where \mathbf{r} is the time-dependent residual vector given in equation 1. The last term in J is included to ensure accurate estimates during the Valsalva maneuver. Figure 1f displays the model fit to heart rate data.

Appendix B.

This appendix describes the implementation of approximating the integrands for equations (23)-(26). We employed estimators proposed by Saltelli et al. [37]. Let $i = 1, \dots, p$ for p the number of parameters, t_j be a time point where $j = 1, \dots, N$ for N the total number of discretized time points, and $l = 1, \dots, L$ be the index of L model function evaluations. Also, $t_1 = 0$ and $t_N = T$ for T the end time point. We approximate the numerator for equation (21) and the integrands for the numerators of equations (23) and (25) as

$$\mathbb{V}_{\theta_i}(\mathbb{E}_{\theta_{\sim i}}[f(t_j; \cdot) | \theta_i]) \approx \frac{1}{L} \sum_{l=1}^L f(t_j, \mathbf{B})_l (f(t_j, \mathbf{A}_{\mathbf{B}}^{(i)})_l - f(t_j, \mathbf{A})_l) \quad (\text{A.1})$$

and the numerator for equation (22) and the integrands for the numerators of equations (24) and (26) as

$$\mathbb{E}_{\theta_{\sim i}}(\mathbb{V}_{\theta_i}(f(t_j; \cdot) | \theta_{\sim i})) \approx \frac{1}{2L} \sum_{l=1}^L f(t_j, \mathbf{A})_l (f(t_j, \mathbf{A})_l - f(t_j, \mathbf{A}_{\mathbf{B}}^{(i)})_l)^2, \quad (\text{A.2})$$

where \mathbf{A} and \mathbf{B} are two independent sampling matrices determined quasi-randomly using Sobol' sets. The matrix $\mathbf{A}_B^{(i)}$ contains all of the columns of \mathbf{A} except the i^{th} column, which is swapped with the i^{th} column of \mathbf{B} . The denominators for equations (21) and (22) and the integrands of the denominators of (23)-(26) were approximated using the variance function `var` in MATLAB® 2019b. Further information on these computational methods can be found in Saltelli et al. [37].

References

References

- [1] A. Alexanderian, P. A. Gremaud, R. C. Smith. Variance-based sensitivity analysis for time-dependent processes. *Reliab Eng Syst Safe*, 196: 1–17. 2020. DOI: 10.1016/j.ress.2019.106722.
- [2] A. Alexanderian, J. Winokur, I. Sraj, A. Srinivasa, M. Iskandarani, W. C. Thacker, O. M. Knio. Global sensitivity analysis in an ocean general circulation model: a sparse spectral projection approach. *Comput Geosci*, 16 (3): 757–778. 2012. DOI: 10.1007/s10596-012-9286-2.
- [3] B. Besselink, U. Tabak, A. Lutowska, N. van de Wouw, H. Nijmeijer, D. J. Rixen, M. E. Hochstenbach, W. H. A. Schilders. A comparison of model reduction techniques from structural dynamics, numerical mathematics, and systems and control. *J Sound Vib*, 332 (19): 4403–4422. 2013. DOI: 10.1016/j.jsv.2013.03.025.
- [4] W. F. Boron, E. L. Boulpaep. *Medical Physiology: A Cellular and Molecular Approach*. 3rd Edition, Elsevier Inc., Philadelphia, PA, 2017. ISBN: 978-1455743773.
- [5] K. P. Burnham, D. R. Anderson. *Model selection and multimodel inference: a practical information-theoretic approach*. 2nd Edition, Springer-Verlag, New York, 2002. DOI: 10.1007/b97636.
- [6] M. Calvo, V. Le Rolle, D. Romero, N. Behar, P. Gomis, P. Mabo, A. I. Hernandez. Global sensitivity analysis of a cardiovascular model for the study of the autonomic response to head-up tilt testing. in: *Conf Proc IEEE Eng Med BiolSoc*, 5458–5461. 2018. DOI: 10.1109/EMBC.2018.8513536.
- [7] L. M. Ellwein, H. T. Tran, C. Zapata, V. Novak, M. S. Olufsen. Sensitivity analysis and model assessment: mathematical models for arterial blood flow and blood pressure. *Cardiovasc Eng* 8 (2): 94–108. 2008. DOI: 10.1007/s10558-007-9047-3.
- [8] F. N. Fritsch, R. E. Carlson. Monotone piecewise cubic interpolation. *SIAM J Numer Anal* 17 (2): 238–246. 1980. DOI: 10.1137/0717021.
- [9] N. Guglielmi, E. Hairer. Implementing Radau IIA methods for stiff delay differential equations. *Computing* 67 (1): 1–12. 2001. DOI: 10.1007/s006070170013.
- [10] J. E. Hall. *Guyton and Hall Textbook of Medical Physiology*. 13th Edition, Elsevier, Inc, Philadelphia, PA, 2016. ISBN: 978-1-4557-7005-2.
- [11] W. F. Hamilton, R. A. Woodbury, H. T. Harper, Jr. Arterial, cerebrospinal and venous pressures in man during cough and strain. *Am J Physiol* 141 (1): 42–50. 1944. DOI: 10.1152/ajplegacy.1944.141.1.42.

- [12] J. L. Hart. *Extensions of global sensitivity analysis: theory, computation, and applications*. Ph.D. thesis, North Carolina State University. 2018.
- [13] J. L. Hart, P. A. Gremaud, T. David. Global sensitivity analysis of high-dimensional neuroscience models: an example of neurovascular coupling. *Bull Math Biol* 81: 1805–1828. 2019. DOI: 10.1007/s11538-019-00578-0.
- [14] B. Iooss, P. Lemaitre. A review on global sensitivity analysis methods. in: *Uncertainty Management in Simulation-Optimization of Complex Systems: Algorithms and Applications*. Research/Computer Science Interfaces Series, Springer, Boston, MA, 59: 101–122. 2015. DOI: 10.1007/978-1-4899-7547-8_5
- [15] A. D. Jose, D. Collison. The normal range and determinants of the intrinsic heart rate in man. *Cardiovasc Res* 4 (2): 160–167. 1970. DOI: 10.1093/cvr/4.2.160.
- [16] F. Kappel, M. Munir. Generalized sensitivity functions for multiple output systems. *J Inverse Ill-Posed Probl* 25 (4): 499–519. 2017. DOI: 10.1515/jiip-2016-0024.
- [17] C. T. Kelley. *Iterative Methods for Optimization*. Frontiers in Applied Mathematics, Society for Industrial and Applied Mathematics, Philadelphia, PA. 1996. DOI: 10.1137/1.9781611970920.
- [18] A. Kiparissides, S. S. Kucherenko, A. Mantalaris, E. N. Pistikopoulos. Global sensitivity analysis challenges in biological systems modeling. *Ind Eng Chem Res* 48 (15): 7168–7180. 2009. DOI: 10.1021/ie900139x.
- [19] P. I. Korner, A. M. Tonkin, J. B. Uther. Reflex and mechanical circulatory effects of graded Valsalva maneuvers in normal man. *J Appl Physiol* 40 (3): 434–440. 1976. DOI: 10.1152/jappl.1976.40.3.434.
- [20] S. A. Kosinski, B. E. Carlson, S. L. Hummel, R. D. Brook, D. A. Beard. Computational model-based assessment of baroreflex function from response to Valsalva maneuver. *J Appl Physiol* 125 (6): 1944–1967. 2018. DOI: 10.1152/japplphysiol.00095.2018.
- [21] V. Le Rolle, A. I. Hernandez, P. Y. Richard, G. Carrault. An autonomic nervous system model applied to the analysis of orthostatic tests. *Model Simul Eng* 2008: 1–15. 2008. DOI: 10.1155/2008/427926.
- [22] K. G. Link, M. T. Stobb, J. Di Paola, K. B. Neevees, A. L. Fogelson, S. S. Sindi, K. Leiderman. A local and global sensitivity analysis of a mathematical model of coagulation and platelet deposition under flow. *PLoS One* 13 (7): 1–38. 2018. DOI: 10.1371/journal.pone.0200917.
- [23] K. Lu, J. W. Clark Jr., F. H. Ghorbel, D. L. Ware, A. Bidani. A human cardiopulmonary system model applied to the analysis of the Valsalva maneuver. *Am J Physiol Heart Circ Physiol* 281 (6): H2661–H2679. 2001. DOI: 10.1152/ajpheart.2001.281.6.H2661.
- [24] G. Mader, M. S. Olufsen, A. Mahdi. Modeling cerebral blood flow velocity during orthostatic stress. *Ann Biomed Eng* 43 (8): 1748–1758. 2015. DOI: 10.1007/s10439-014-1220-4.
- [25] A. Mahdi, J. Sturdy, J. T. Ottesen, M. S. Olufsen. Modeling the afferent dynamics of the baroreflex control system. *PLoS Comput Biol* 9 (12): 1–18. 2013. DOI: 10.1371/journal.pcbi.1003384.

- [26] S. Marino, I. B. Hogue, C. J. Ray, D. E. Kirschner. A methodology for performing global uncertainty and sensitivity analysis in systems biology. *J Theor Biol* 254 (1): 178–196. 2008. DOI: 10.1016/j.jtbi.2008.04.011.
- [27] A. D. Marquis, A. Arnold, C. Dean-Bernhoft, B. E. Carlson, M. S. Olufsen. Practical identifiability and uncertainty quantification of a pulsatile cardiovascular model. *Math Biosci* 304: 9–24. 2018. DOI: 10.1016/j.mbs.2018.07.001.
- [28] M. D. Morris. Factorial sampling plan for preliminary computational experiments. *Technometrics* 33 (2): 161–174. 1991. DOI: 10.2307/1269043.
- [29] C. H. Olsen, J. T. Ottesen, R. C. Smith, M. S. Olufsen. Parameter subset selection techniques for problems in mathematical and biology. *Biol Cybern* 113 (1-2): 121–138. 2019. DOI: 10.1007/s00422-018-0784-8.
- [30] M. S. Olufsen, J. T. Ottesen. A practical approach to parameter estimation applied to model predicting heart rate regulation. *J Math Biol* 67 (1): 39–68. 2013. DOI: 10.1007/s00285-012-0535-8.
- [31] M. S. Olufsen, J. T. Ottesen, H. T. Tran, L. M. Ellwein, L. A. Lipsitz, V. Novak. Blood pressure and blood flow variation during postural change from sitting to standing: model development and validation. *J Appl Physiol* 99 (4): 1523–1537. 2005. DOI: 10.1152/japplphysiol.00177.2005.
- [32] M. S. Olufsen, H. T. Tran, J. T. Ottesen, L. A. Lipsitz, V. Novak. Modeling baroreflex regulation of heart rate during orthostatic stress. *Am J Physiol Regul Integr Comp Physiol* 291 (5): R1355–R1368. 2006. DOI: 10.1152/ajpregu.00205.2006.
- [33] S. R. Pope, L. M. Ellwein, C. Zapata, V. Novak, C. T. Kelley, M. S. Olufsen. Estimation and identification of parameters in a lumped cerebrovascular model. *Math Biosci Eng* 6 (1): 93–115. 2009. DOI: 10.3934/mbe.2009.6.93.
- [34] M. U. Qureshi, M. J. Colebank, L. M. Paun, L. Ellwein Fix, N. Chesler, M. A. Haider, N. A. Hill, D. Husmeier, M. S. Olufsen. Hemodynamic assessment of pulmonary hypertension in mice: a model-based analysis of the disease mechanism. *Biomech Model Mechanobiol* 18 (1): 219–243. 2019. DOI: 10.1007/s10237-018-1078-8.
- [35] E. B. Randall, A. Billeschou, L. S. Brinth, J. Mehlsen, M. S. Olufsen. A model-based analysis of autonomic nervous function in response to the Valsalva maneuver. *J Appl Physiol* 127 (5): 1386–1402. 2019. DOI: 10.1152/japplphysiol.00015.2019.
- [36] E. B. Randall, N. Z. Randolph, M. S. Olufsen. Persistent instability in a nonhomogeneous delay differential equation system of the Valsalva maneuver. *Math Biosci* 319: 108292. 2019. DOI: 10.1016/j.mbs.2019.108292.
- [37] A. Saltelli, P. Annoni, I. Azzini, F. Campolongo, M. Ratto, S. Tarantola. Variance based sensitivity analysis of model output. Design and estimator for total sensitivity index. *Comput Phys Commun* 181 (2): 259–270. 2010. DOI: 10.1016/j.cpc.2009.09.018.
- [38] R. C. Smith. *Uncertainty quantification: theory, implementation, and applications*. Society for Industrial and Applied Mathematics (SIAM), Philadelphia, PA. 2014. ISBN: 978-1611973211.

- [39] T. J. Snowden, P. H. van der Graaf, M. J. Tindall. Model reduction in mathematical pharmacology. *J Pharmacokinet Pharmacodyn* 45 (4): 537–555. 2018. DOI: 10.1007/s10928-018-9584-y.
- [40] I. M. Sobol. Sensitivity estimates for nonlinear mathematical models. *Math Mod Comp Exp* 1 (4): 407–414. 1993.
- [41] I. M. Sobol. Global sensitivity indices for nonlinear mathematical models and their Monte Carlo estimates. *Math Comput Simul* 55 (1-3): 271–280. 2001. DOI: 10.1016/S0378-4754(00)00270-6.
- [42] I. M. Sobol, S. S. Kucherenko. Derivative based global sensitivity measures. *Procedia Soc Behav Sci* 2 (6): 7745–7746. 2010. DOI: 10.1016/j.sbspro.2010.05.208.
- [43] C. B. Storlie, J. C. Helton. Multiple predictor smoothing methods for sensitivity analysis: description of techniques. *Reliab Eng Syst Safe* 93 (1): 28–54. 2008. DOI: j.ress.2006.10.012.
- [44] T. Sumner, E. Shephard, I. D. L. Bogle. A methodology for global sensitivity analysis of time-dependent outputs in systems biology modelling. *J R Soc Interface* 9 (74): 2156–2166. 2012. DOI: 10.1098/rsif.2011.0891.
- [45] D. Valdez-Jasso, H. T. Banks, M. A. Haider, D. Bia, Y. Zocalo, R. L. Armentano, M. S. Olufsen. Viscoelastic models for passive arterial wall dynamics. *Adv Appl Math Mech* 1 (2): 151–165. 2009.
- [46] L. H. Weimer. Autonomic testing: common techniques and clinical applications. *Neurologist* 16 (4): 215–222. 2010. DOI: 10.1097/NRL.0b013e3181cf86ab.
- [47] E. Wit, E. ven den Heuvel, J.-W. Romeijn. All models are wrong : an introduction to model uncertainty. *Stat Neerl* 66: 217–236. 2012. DOI: 10.1111/j.1467-9574.2012.00530.x.